Development of Surgical Navigation System

for Less Invasive Therapy

of Intervertebral Disk Disease

Sangseo Jeon （전 상 서 全 商 瑞）

Department of Robotics Engineering
로봇공학전공

DGIST

2014

Master's Thesis

석사 학위논문

Development of Surgical Navigation System

for Less Invasive Therapy

of Intervertebral Disk Disease

Sangseo Jeon (전 상 서 全 商 瑞)

Department of Robotics Engineering

로봇공학전공

DGIST

2014

Development of Surgical Navigation System
for Less Invasive Therapy
of Intervertebral Disk Disease

Advisor	:	Professor Jaesung Hong
Co-advisor	:	Professor Minyoung Kim

By

Sangseo Jeon
Department of Robotics Engineering
DGIST

A thesis submitted to the faculty of DGIST in partial fulfillment of the requirements for the degree of Master of Science in the Department of Robotics Engineering. The study was conducted in accordance with Code of Research Ethics[1]

01. 10. 2014

Approved by

Professor	Jaesung Hong (Advisor)	(Signature)
Professor	Minyoung Kim (Co-Advisor)	(Signature)

Development of Surgical Navigation System

for Less Invasive Therapy

of Intervertebral Disc Disease

Sangseo Jeon

Accepted in partial fulfillment of the requirements
for the degree of Master of Science.

12. 05. 2013

Head of Committee	Prof. Jaesung Hong	(인)
Committee Member	Prof. Minyoung Kim	(인)
Committee Member	Prof. Pyunghun Chang	(인)

ABSTRACT

Epiduroscopy (EDS) is an emerging branch of less invasive treatment of chronic back pain and lumber herniated intervertebral disc disease. However, the EDS leads to X-ray radiation exposure and contrast agent-induced nephrotoxicity, since it is usually performed under the guidance of fluoroscopy. In this regard, We propose a new surgical navigation system for the EDS, which uses an electromagnetic tracking system (EMTS) and an optical tracking system (OTS) in a complementary way to compensate for inherent tacking inaccuracy of the EMTS and finally improve the navigation accuracy. The proposed system aims at replacing the conventional fluoroscopy to reduce the radiation doses and providing 3D visual information to help surgeons more easily understand the surgical situation. For further improvement in the navigation accuracy of the proposed system, correction for magnetic field distortion based on the polynomial fitting technique are also studied. The phantom experiments were performed to quantitatively evaluate the accuracy of the proposed system and qualitative assessment was also performed with clinical application of the system over 14 patients.

Keywords: Epiduroscopy, Surgical Navigation, Magnetic Field Distortion, Calibration, Registration

Contents

List of Tables

List of Figures

Ⅰ. INTRODUCTION

1.1 Brief Anatomy of the Spine and vertebrae

The spine, also known as the vertebral column or spinal column, is a column consisting of a series of bones called vertebrae. Each pair of vertebrae is connected by a flexible intervertebral disc with the exception of ones in the sacral and coccygeal regions -they become united in the adulthood to form two single bones: the sacrum and the coccyx-, thus enabling the spine to be bent flexibly. There are usually thirty-three vertebrae in the spine, which are divided into cervical, thoracic, lumbar, sacral and coccygeal regions. As shown on Fig 1.1, there are seven vertebrae in the cervical region, twelve in the thoracic, five in the lumbar, five in the sacral and four in the coccygeal. At times, these numbers are varied by an extra vertebra in one region, usually compensated by a missing one in other region. However, the number of cervical vertebrae hardly ever changes. Vertebrae are named by using a first letter of the name of the regions –C for cervical region, T for thoracic, L for lumbar and S for sacral- and a number which is ordered from head to feet.

With the exception of the first two cervical vertebrae –C1 and C2, also known as atlas and axis- movable vertebrae share some common features as the one depicted on Fig 1.2. They consist of two parts: an anterior segment or body and a posterior one known as vertebral or neural arch. These enclose the spinal canal or vertebral foramen, which serves as a protection for the spinal cord. The vertebral body (corpus vertebrae) is the largest part of the vertebrae and is more or less cylindrical in its shape. Its upper and lower surfaces are flattened and rough and give attachment to the intervertebral fibrocartilages. Vertebrae are connected to each other by their bodies, forming a strong pillar for the support of the head and trunk.

The vertebral arch is formed by a pair of pedicles and seven bony extrusions or processes which serve as attachment of muscles and ligaments. All bony parts of the vertebrae are composed of cancellous tissue enclosed by a layer of the more compact cortical bone. Cortical coating are thinner in the vertebral body, whereas it is considerably thicker in the vertebral arch and processes.

The pedicles are two short and thick processes projected backwards, one from each side of the vertebral body. They are connected to the laminae, a pair of broad plates directed backwards and medialward, which fuse in the medial line completing the posterior side of the vertebral foramen, also shown on Fig 1.2.
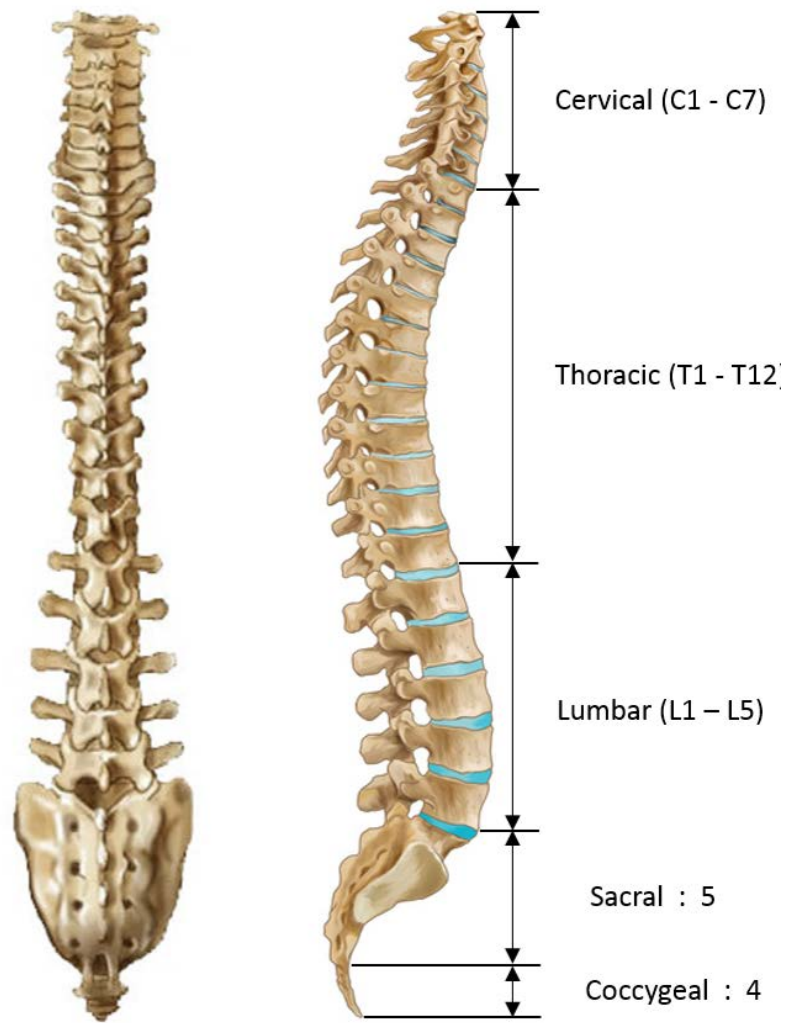
Figure 1.1 Posterior view (left) and lateral view (right) of the human spine, consisting of the cervical (C), thoracic (T), lumbar (L), sacral and coccygeal regions.
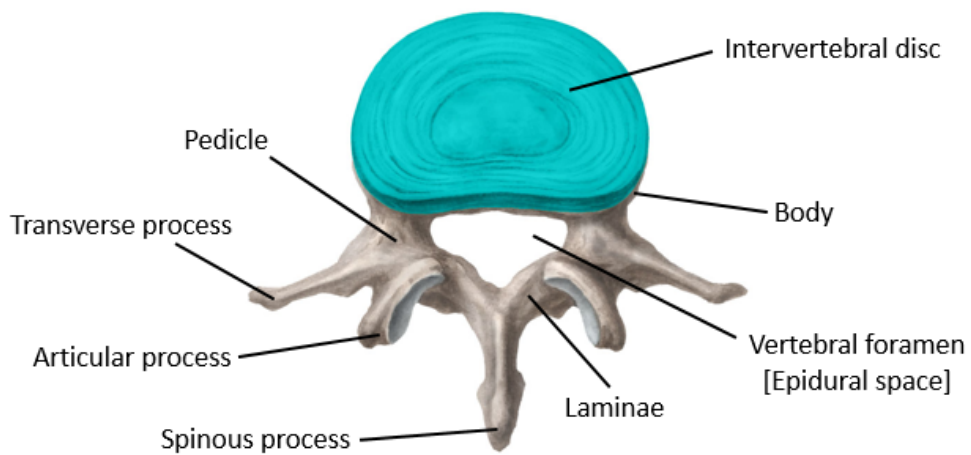
Figure 1.2 Cross-sectional view of a vertebra and an intervertebral disc.

1.2 Conventional procedure: its limitations and related research

Although the underlying mechanisms of chronic refractory low back pain (LBP) have not been fully investigated, its pathophysiology has been addressed in clinical, as well as research fields by applying a range of treatment methods from conservative therapy to surgical approach. In particular, surgical treatment has been one of the most common approach for patients with refractory LBP (e.g. intervertebral disc hernia in the lumbar spinal region and lumbar spinal stenosis).

However, chronic LBP treatment options are limited for patients who have received surgical treatment more than once. Repeated surgery for lesions which are not clearly seen on magnetic resonance imaging (MRI) often causes difficulty in making an accurate diagnosis. To address the above limitations, spinal surgeons have been paying increasing attention to epiduroscopy (EDS).

EDS is a percutaneous minimally invasive endoscopic examination of the epidural space that allows visualization of normal anatomical structures in the spinal region such as the dura mater, blood vessels, connective tissue, nerves and fatty tissue as well as pathological structures such as adhesions, sequesters, inflammatory processes and fibrosis. EDS was first introduced in 1931 by Burmann who examined the epidural space via endoscopy [1]. Recently, EDS can also be used for therapeutic inventions due to the development of a working channel scope allowing a laser fiber or other working tools to be inserted and used to enhance the effectiveness of surgery [2]. Epiduroscopic laser disc and neural decompression (ELND) is one of the emerging interventions which show such therapeutic use of EDS. ELND is a less invasive procedure for laser ablation of the target lesion with guidance of the endoscopic view and fluoroscopic images from a C-arm unit -depicted on Fig 1.3- to treat LBP or lumbar herniated intervertebral disc disease.

In ELND, a steerable video-guided catheter –shown on Fig 1.4- is inserted through a small incision around the sacral area of patients and advanced through the epidural space to reach the target lesion area with the fiber endoscope and the laser-emitting fiber within its working channels. ELND offers a great deal of advantages over highly invasive surgeries including smaller postoperative scars, less blood loss, minimal likelihood of infection, reduced operating time, and early return to daily life. Kim et al. [3] reported the clinical outcomes of 20 epiduroscopic neural decompression (END) patients, and 78 ELND patients. According to the study, eighty-two percent of the patients treated with ELND reported positive treatment results and thus ELND is judged to be an effective therapeutic modality for patients with chronic refractory LBP. Choi et al. [4] also presented in their follow-up

study after the performance of the EDS on 24 patients that percutaneous EDS is an effective technique to diagnose and treat the failed back pain syndrome.
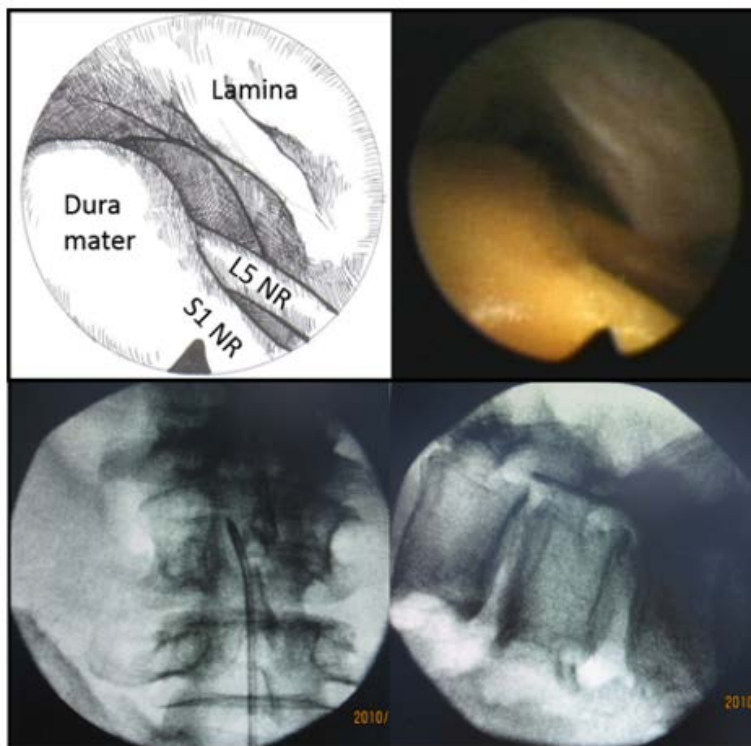
Figure 1.3 Endoscopic view and fluoroscopic images in coronal and lateral planes.
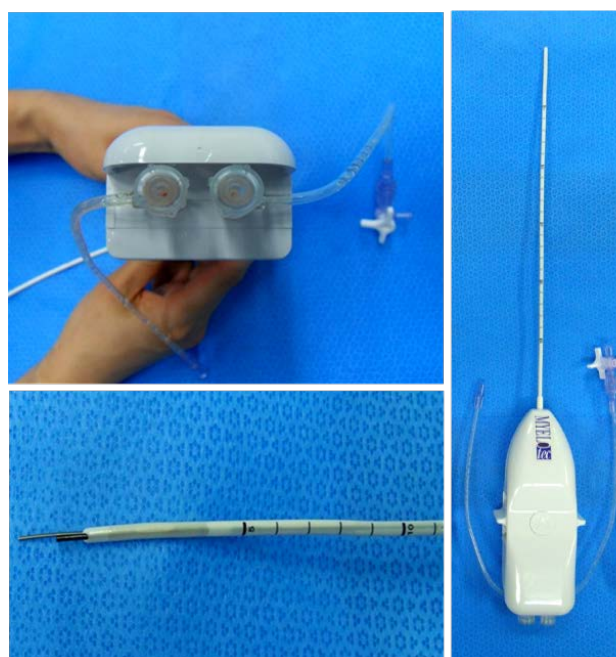
Figure 1.4 Steerable catheter with two working channels allowing working tools such as a laser-emitting fiber and fiber endoscope to be inserted.
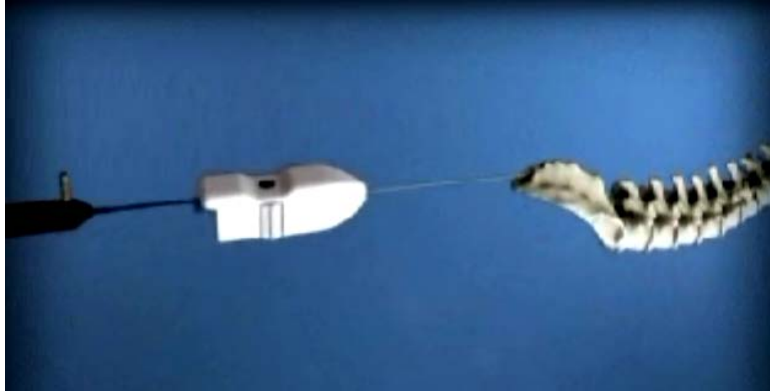
Figure 1.5 Conceptual figure showing epiduroscopic procedure.

Despite the fact that EDS is an effective procedure for treatment of LBP patients, and also offers the afore-mentioned advantages over highly invasive surgery, a couple of critical problems limit its application in the medical field at times.

Surgeons perform epiduroscopic procedures while observing patient's anatomical structures with the endo-scopic view from the flexible fiberscope. Endoscopy is an effective imaging modality in that it offers direct view of the anatomical structures inside the patient body, as shown on Fig 1.3. However, in case of the flexible fiber-scope, its narrow field of view (FOV) and relatively low resolution could hinder operators from accurately local-izing and placing the catheter tip inside the patient body. Thus, during the whole procedure, surgeons should be provided with a considerable amount of fluoroscopic images as well as endoscopic images [5].

Fluoroscopy -it is a branch of x-ray imaging, but is different from x-ray imaging in that it can provide con-tinuous images reflecting structural change of the anatomy in real time- generates a medical image by using not only X-ray radiation, but also contrast agent for the purpose of enhancing the contrast of structures or fluids within the body which are visualized in the image. In this regard, a surgical patient is likely to suffer from post-operative side effects resulting from exposure to high radiation doses and possible contrast agent-induced adverse reactions [5-6].

In fact, the problem of high radiation dose is even worse for clinical steps or surgeons rather than a surgical patient, considering that surgeon could perform several procedures even per week while patients might have a few number of procedures at most for their life time. Komiya et al. [7] has presented a study of radiation exposure in the performance of epiduroscopy. In the study, they measured the radiation dose during a 10-minute fluoros-

copy exposure in humanoid models and the duration of fluoroscopy during the clinical epiduroscopy in 14 patients. With the average operating time of 50 minutes and the average fluoroscopic time of 9 minutes and 26 seconds, they reported that radiological dosages were less than the threshold doses that could lead to organ injuries for one epiduroscopic procedure, but care should be taken for cumulative radiation exposures in repeated procedures, which could be an important aspect in terms of operating surgeons.

A preventive measure to minimize radiation dose in the operating room is to wear a lead apron of not less than 0.25 mm of lead equivalent in case of operating surgeons [8]. However, its huge weight –approximately 7 kg- could restrict movements of operating surgeons. According to Khalil et al [9], the weight of a lead apron could induce a pressure of 300lbs per square inch on the intervertebral disc spaces, which, in turn, could be the provoking mechanism of LBP among operating surgeons [10]. In addition, putting on a lead apron not only could increase on risk of contamination, but is also time consuming. To address such problems, Lee et al [11] has proposed a radiation protection method for the operating room, which is based on a movable sterile shield being wheeled into the operative field and positioned between the surgeon and the operating table in time of X-ray imaging. In terms of duration of radiation exposure, intermittent use of fluoroscopic imaging in pulse mode during the EDS procedure has been proposed as an alternative for radiation exposure [12]. However, it not only gives still considerable amount of X-ray radiation, but also leads to loss of image resolution, providing inconvenience to operators in terms of understanding the current surgical situation. When it comes to the surgical patients, gonadal shielding should be used for all patients getting X-ray radiation, but, in case of the EDS procedure, gonadal shielding for the surgical patient is excluded since it highly interferes with the procedure.

Figure 1.6 Lead apron (left) and movable sterile shield presented by Lee et al [11] (right).

Basically, a C-arm unit provides only two-dimensional (2D) fluoroscopic images to surgeons, which induces consequent lack of depth perception, making it difficult for surgeons to effectively estimate three-dimensional (3D) anatomical structure of the surgical patient. In recent times, a G-arm unit has been developed to address the problem and popularized in the medical field. A C-arm unit has a pair of X-ray source and receptor, geometry of which is in the shape of alphabet C. It can be rotated about surgical bed by almost random angles, but generate an image on only one plane.

On the other hand, a G-arm unit has two pairs of X-ray source and receptor with the shape of alphabet G. The central axes of each pair are at right angle, which means that it can generate two images in two orthogonal planes at one time and consequently facilitates surgeon's understanding of the anatomical structure of the patient. However, in case of using a G-arm unit, the radiation dose for both the patient and surgeons naturally increases two times compared to that from a C-arm unit. In addition, combining two orthogonal images and figuring out the resultant 3D position of the structure is done by relying on personal competence of each surgeon, thus requiring a great deal of training experiences [13].

1.3 Goal of the Thesis

The aim of this study is to develop a surgical navigation system for assisting orthopedic surgeons in the epiduroscopic procedure by replacing fluoroscopy in part to reduce X-ray radiation doses for both the surgical patient and surgeons, and providing surgeons with accurate visual information to help them understand the current surgical situation.

The practical aspects of the clinical application as well as the acceptable navigation accuracy should be also considered in the development of the proposed system.

1.4 Thesis Outline

This thesis is organized on seven chapters.

Chapter 1 is the current part which presents the introduction to EDS and the brief anatomy of its surgical target site, limitations of the conventional procedure and the related research, and the brief overview of the proposed system.

Chapter 2 describes fundamental components for the surgical navigation which is the background knowledge for figuring out the proposed system as well as the specific description of the proposed system including the configuration of the electromagnetic navigation system, hybrid navigation system, compensation of electromagnetic field distortion for further improvement of the navigation accuracy, and the developed software for the proposed system.

Chapter 3 describes the materials and the experimental setup to evaluate the accuracy of the proposed system.

Chapter 4 describes the experimental results. The navigation accuracies of the electromagnetic navigation system, the hybrid navigation system, and the hybrid navigation system with electromagnetic distortion compensation are compared in terms of fiducial registration error and target registration error.

Chapter 5 describes the clinical application of the proposed system. The flows of the conventional procedure and the surgical navigation-guided procedure, crucial considerations for each step of the procedure, and discussion after clinical trials are included.

Chapter 6 describes discussions on limitations as well as excellence of the proposed system.

In conclusion, summary of the study and future works are presented on Chapter 7.

Ⅱ. Surgical Navigation System for Epiduroscopic Procedure

2.1 Basics

The followings provide fundamental background knowledge required to understand the proposed navigation system prior to detailed description of the system.

2.1.1 Surgical Navigation

Surgical navigation stands for surgical guidance technique based on medical images of the surgical patient. It can be likened to the vehicle navigation system which uses global positioning system (GPS) navigation device. In surgical navigation, surgical instruments correspond to the vehicle, a position tracking system to the satellite, and medical images to the road map. As the vehicle navigation gives information on where the vehicle is now and which direction it should go in to reach the destination, surgical navigation performs similar things by displaying the position of the surgical instrument relative to the patient anatomy on CT, MR or ultrasound images, which helps surgeons approach the target lesion quickly without damaging other important organs near the surgical target. To use medical images as a guidance map in surgical navigation as mentioned above, patient-to-image registration is required, which is a process to match the coordinate systems of the patient, or tracked object in the real world and the medical image of the patient. Accurate patient-to-image registration is a key issue to successful IGS procedure.

Surgical navigation is most helpful in case that the target lesions are located inside or behind the organ and thus invisible with naked eyes or endoscopic view. Especially, in terms of safety, functionality of warning navigation may be useful in avoiding complications arising from invisibility of the surgical target, which provides some quantitative information like distance between the surgical tool and the invisible target in real time or some warning sound in case that the surgical tool closely approaches the important normal organ located near the surgical target beyond the pre-defined distance limitation. The medical image guidance is also helpful for the case where the boundary between tumor and normal tissue is vague. That complication can be solved by surgeons referring to the virtual tumor object segmented from the medical images on the navigation display.

In terms of visualization method, surgical navigation can be categorized into two groups. The first one is virtual reality (VR)-based surgical navigation. In VR-based navigation, both surgical instruments and the patient anatomy are displayed in the 3D virtual space on the navigation display. Surgeons are able to understand the surgical situation with ease in that the positional relationship between the tool and the patient anatomy can be observed from various viewpoints via simple user interaction with the navigation system. Such functionality alleviates in part the lack of depth perception stemming from use of the 2D display device. On the other hand, surgeons could experience inconvenience in using VR navigation system in that they have to turn their eyes from the patient body, or the surgical site to the navigation monitor so as to refer to navigation information.

The other type of surgical navigation is augmented reality (AR)-based one. In AR navigation, navigation information including virtual objects segmented from the medical images is superimposed on the real-time endoscopic or microscopic image. The fact that surgeons don't need to turn their eyes to the separate navigation monitor to obtain navigation information is one of advantages of AR-based navigation over VR-based one. In addition, surgeons can feel more sense of reality from the AR navigation view since they are provided with images showing real anatomical structure of the surgical patient as well as additional navigation information. However, depending on surgical procedures, superimposed objects on the endoscopic view could hinder surgeons from normal observation of pure anatomical structure or the surgical tool. For reliable accuracy of AR navigation, cumbersome processes must be intra-operatively performed with high accuracy including camera calibration essential for quantitative use of camera images with position tracking information and camera registration between the camera coordinate frame and the position tracker frame, which impedes the applicability of AR navigation in the medical field.

In addition to visualization method, there are several criteria including imaging modalities, tracking modalities, or software platforms which determine the types of surgical navigation. In the following sections, overviews of the aforementioned things are provided.

2.1.2 Tracking Modality

In image-guided surgery (IGS) applications, tracking systems are used to track surgical tools and the anatomy of the surgical patient, providing surgeons with information on positional relationship between them. Intraoperative use of tracking systems are essential for surgical navigation and their tracking accuracy should be guaranteed to be reliable depending upon the required surgical precision in different surgical procedures. Among

a multitude of tracking modalities, optical tracking systems (OTS) and electromagnetic tracking systems (EMTS) are the most common and popular for IGS applications. The followings will briefly describe currently available tracking modalities.

Optical Tracking System

Optical tracking system (OTS) is one of the most prevalent tracking systems used for IGS applications. The OTS falls into two primary classes. One is active type and the other is passive one. An active system tracks pose of the target object by flashing a set of infrared LED markers attached to the target and identifying the pattern or firing sequence of the markers. In case of a passive system, infrared rays are emitted from the light source and the stereo camera receives the rays reflected from the retro-reflective markers attached to the target object. In addition, there exists another type of a passive system which picks up a certain pattern with a stereo camera without using retro-reflective markers. The active type system presents better performance than the passive type, but its wired connection from the system to the marker set limits use in complicated surgical environments. The OTS is most common in the surgical navigation area in that it provides reliable accuracy. However, the OTS has a huge limitation that it suffers line-of-sight problem. In other words, it cannot normally work if the infrared rays are blocked by obstacles located between the camera and the markers. Another limitation of the OTS is that it cannot be used to track flexible instruments, the tool tip location of which could be changed with respect to the attached marker frame in real time.

Electromagnetic Tracking System

Electromagnetic tracking system (EMTS) determines the pose of a coil sensor, or receiver relative to that of a magnetic field generator (FG), or transmitter in real time. The FS consists of three orthogonal coils generating corresponding orthogonal electromagnetic fields in each measurements cycle. The sensor senses the generated fields, and then position and orientation of the sensor are computed based on the measured electrical signals and a physical model of the magnetic field [14]. At this point, the sensor is required to be placed in the magnetic field generated from the transmitter and be connected to the system control unit through a wire. Tracking data is usually provided as translation vectors for positional measurements and Euler angles, or quaternions for ori-entation information, which is also the same case in OTS. The obvious advantage of the EMTS is that it does

not suffer from line-of-sight constraint between the FS and the sensor like the OTS does, which means the EMTS allows the coil sensor to be attached to surgical instruments including a flexible catheter or endoscope, and be tracked inside the human body. However, the EMTS has a relatively small tracking volume compared with that of the OTS. Moreover, anything that distorts the generated magnetic field from the FG such as metallic structure or other local magnetic field could decrease the tracking accuracy of the EMTS. Excluding existence of metallic structure or any magnetic interference, the measurement error of the EMTS increases proportionally to the fourth power of the distance between the FG and the sensor [15]. In comparison to the OTS, the tracking accuracy of the EMTS is at one order of magnitude lower level.

Figure 2.1 Optical tracking system (OTS) and electromagnetic tracking system (EMTS).

Real-time Imaging

Although not acting as a stand-alone tracking system, a further method of tracking is the use of medical imaging directly. A good example would be the use of fluoroscopy or ultrasound, where a fiducial pattern can be located in the image, and based on that information a registration can be made between the tool and anatomy. Typical modalities that lend themselves to real-time tracking are CT fluoroscopy and MRI. Sometimes, the use of real-time imaging is combined with a stand-alone tracking system. The examples include an optically tracked fluoroscope head, and a calibrated and electromagnetically tracked ultrasound probe used for 3D ultrasound imaging and robotic needle guidance [16].

Robotic System

A robot is also proven to be a useful tool for localization of a surgical instrument. Although it is not a passive tracking system, an accurately calibrated robot allows the user to very accurately place the end effector of the

robot into the precise location within the calibrated workspace. In that regard, if the robot is being used to assist a surgical procedure, a byproduct of its use is that the tool pose can be relayed to a navigation display to render the IGS scene without any additional tracking means. Integrated Surgical Systems (ISS) Neuromate robot with corresponding IGS software allows for precise manipulation of neurosurgery instruments and replaces the need for any stereotactic frames to be affixed to the patient's skull. A more modern robotic surgery system, Intuitive Surgical's da Vinci robot can be utilized for more general purposes, but is mostly used for abdominal and thoracic procedures.

Laser Ranger

Another method of registration and tracking is accomplished through the use of laser range finders. The devices emit laser light that is reflected back to the device. Based on time-of-flight information, the shape, position, and velocity of a target or surface can be obtained. Such a device is less useful for tracking the pose of a tool, but is proven to be very useful for tracking and mapping a surface to perform surface matching with iterative closest point (ICP) algorithm. The typical use of the laser ranger are found in the 3D Digital system used for cortical shift tracking and the laser ranging system (LRS) for mobile robotics applications. In addition to lasers, ultrasonic and other sources can be similarly used for range finding and tracking.

(a)   (b)
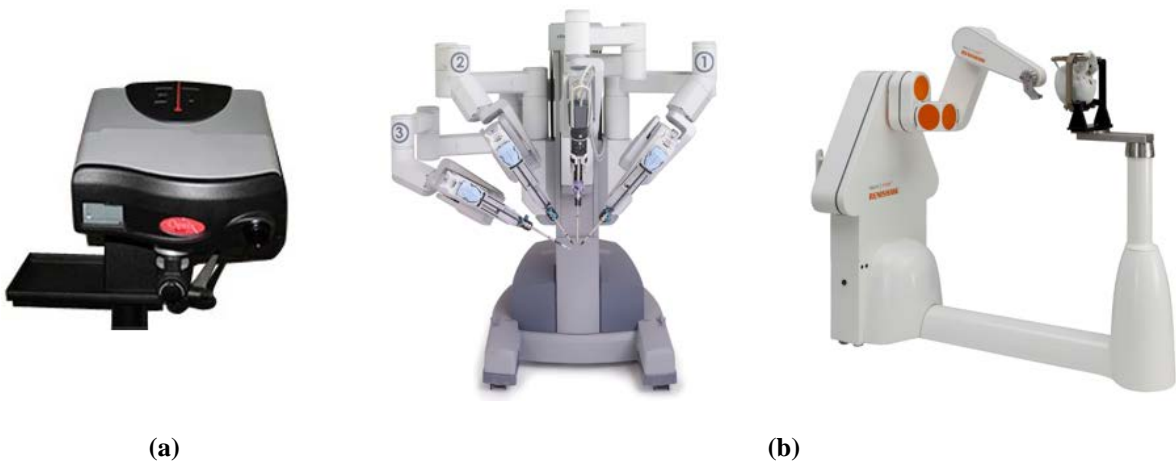
Figure 2.2 (a) Laser scanner and (b) robotic systems used in the medical field.

2.1.3 Imaging Modality

In recent days, different kinds of imaging modality are able to be utilized for surgical navigation. Among many of them, surgeons should select the most suitable one for each surgical procedure, considering distinguishing features of each imaging modality. The followings present an overview of the basic imaging principle and characteristics of each imaging modality.

Computed Tomography

Computed Tomography (CT) is one of the most widely used diagnostic imaging modalities. The imaging principle of CT is basically identical to that of X-ray imaging except that CT provides 3D reconstructed images. In respect that CT imaging uses X-ray, hard tissues including bone are well imaged while soft tissues such as nerve, tendon, or cartilage are not clearly identifiable. The image intensity is determined by the X-ray absorption ratio at different tissues. It enables to obtain a constant image intensity for each tissue or organ, which means that intensity-based image segmentation can be readily implemented with CT images to generate 3D virtual model of the important anatomical structure used for surgical navigation. CT scanning requires relatively short imaging time compared with that of MRI and is seldom limited by image distortion arising from unconscious movements including respiratory movement. The main drawback of CT imaging is exposure to X-ray radiation. For this reason, repetitive CT scanning of one patient should be avoided as far as possible. Radiation problem is even worse for radiologists or surgeons who routinely use intraoperative CT scanning or fluoroscopy. However, for surgical navigation, one additional CT scanning must be performed at a cost of radiation exposure to obtain images where fiducial markers attached to the patient body are included and identified.

Magnetic Resonance Imaging

Magnetic resonance imaging (MRI) is another popular imaging technique used to visualize internal structures of the body in detail. The principle of MRI is based on the movement of protons of hydrogen which are contained in a form of water in the human body. The protons in the body are aligned in a large magnetic field. After that, radio frequency pulse is applied to make the protons fall down their spin axis. Finally, we obtain the reactive signals emitted from the protons while their spin axis is gradually recovered to be in the initially aligned state. MRI is considered to be very safe to the patient in that MRI does not use ionizing radiation unlike CT

scans or traditional X-rays. MRI provides even better contrast for soft tissue than that for hard one because soft one has a lot of water or fat which contains abundant hydrogen. In that regard, MRI is especially useful in imaging the brain, muscles, the heart, and cancers compared with other medical imaging techniques such as CT or X-rays. MRI takes much longer time to obtain the images than CT imaging, which takes several seconds for single 2D slice imaging.   For this reason, the patient must remain stationary during the whole imaging duration, and if the patient moves during the scanning, some image distortion from the movement could tack place and internal anatomy of the patient would not be clearly identifiable in the images. Due to the aforementioned imaging principle of MRI, MRI room has the area limitation that metal or magnetic materials should be located outside of 5 Gauss line that surrounds the MR magnets. Especially, in case of intraoperative MRI, or open MRI in the operating room, that regulation must be strictly obeyed in that a lot of metallic surgical instruments or medical devices exist in the operating room. Basically, metallic instruments should not be carried in the MRI room. However, for intraoperative use of open MRI in the operating room, all surgical instruments required in the procedure could be substituted with instruments made from non-metallic or nonmagnetic material such as ceramic, plastic, or titanium.
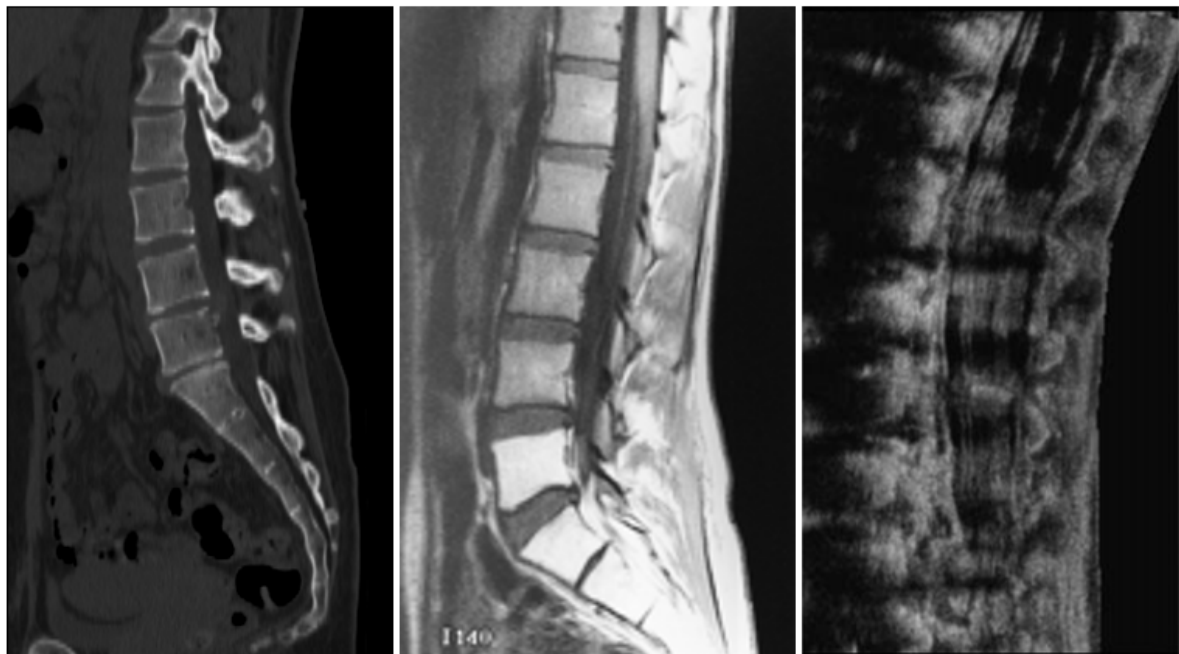
Figure 2.3 Medical images. CT (left), MR (center), and ultrasound (right) image of the human vertebral column.

Ultrasonography

Ultrasonography (US) is an ultrasound-based diagnostic imaging technique used for visualizing subcutaneous body structures including tendons, muscles, joints, vessels and internal organs for possible pathology or lesions. US makes use of amplitude and elapsed time of echo signals to reconstruct 2D images. It is the most safe and nearly harmless imaging modality to the human body. The cost is low and the size is small; therefore, it has been installed in many hospitals and clinics. Another strong advantage of US is the capability of real-time imaging, which is not available in CT or MRI. It also has high sensitivity and resolution, although it has low specificity. We can recognize any suspicious region in the US images, but it is hard to exactly specify what it is. Ultrasound is often used for percutaneous needle insertion therapies such as radio frequency ablation (RFA) or percutaneous ethanol injection therapy (PEIT). These are therapies to insert a needle to the tumor and kill it by heat or ethanol. Surgeons search the tumor and introduce a needle by referring to the US images. Sometimes, the tumor is not clearly identified in 2D US images. In that case, MR or CT images can be used with US images at the same time to find the tumor and guide the needle insertion.

Endoscopic Imaging

Endoscopic surgery has rapidly spread in various area since it is less invasive than conventional open surgery. Pain and scarring is less and an earlier return to daily life is possible. Various endoscopes have been developed. Such as laparoscope for the abdomen area, arthroscope for the orthopedic area, neuroendoscope for neurosurgery, and so on. Latest endoscopes have very small diameter less than 5 mm, and 3D stereo vision is supported in them. There are three kinds of structures for endoscope. The most conventional type uses a relay lens and CCD camera connected to the scope. Another type uses optical fibers instead of a relay lens. The other type uses a distal CCD at the tip of endoscope. The second and third types can be used for flexible endoscopes. The endoscopic image is in color and suitable to observe the organ surface. On the other hand, CT or MR images provide cross-sectional images inside the organ. AR-based surgical navigation displays the endoscopic image and CT or MR image superimposed at the same time, which is described in detail in the next chapter.

2.2 EMTS-based Navigation System

For surgical navigation system assisting ELND procedures, we adopted a commercially available EMTS (Aurora, NDI, Waterloo, Canada). Video-guided catheter used in ELND is a flexible and steerable catheter which has two working channels of 1.3 mm diameter to allow insertion of surgical instruments including a fiber endoscope and a laser fiber. To track the pose of the video-guided catheter, we adopted 5DOF catheter-type magnetic sensor (610017, NDI, Waterloo, Canada) with 1.2 mm diameter and 2 m length. Cumbersome works for integrating a position sensor with the video-guided catheter do not need to be done, being replaced by insertion of the adopted catheter sensor into the working channel of video-guided catheter and placement of the sensor tip at the end of the video-guided catheter. Use of a 6DOF catheter-type sensor could be a good choice in that a 5DOF sensor lacks tracking information of orientation in axial direction. However, the diameter of a 6DOF sensor is larger than that of a 5DOF sensor, which restricts insertion of a 6DOF sensor into the working channel of the video-guided catheter. Furthermore, orientation of the catheter in axial direction is not an important information in surgical navigation for ELND since only the location and direction of the catheter tip are crucial cues for surgeons understanding the surgical situation in ELND. To track pose of the surgical patient, a 6DOF cable sensor (610016, NDI, Waterloo, Canada) was attached to the patient skin as a reference sensor. In ELND navigation, as in the conventional navigation method using a stereotactic frame [17], a patient reference sensor could be omitted in that a surgical patient gets general anesthesia and seldom moves during the whole procedure. However, additional use of a patient reference sensor offers two crucial advantages; Movement from respiration activity of the patient can be tracked and compensated to more accurately estimate the current location of the catheter tip relative to the patient anatomy. In addition, without a reference sensor, patient-to-image registration must be re-conducted in case that position of either the surgical patient or the position tracker is altered after the registration step. In case of performing patient-to-image registration with the patient reference sensor, the surgical patient or the position tracker can be moved freely after the registration since the positional relationship between the patient reference and the catheter does not change. Figure describes patient-to-image registration process.
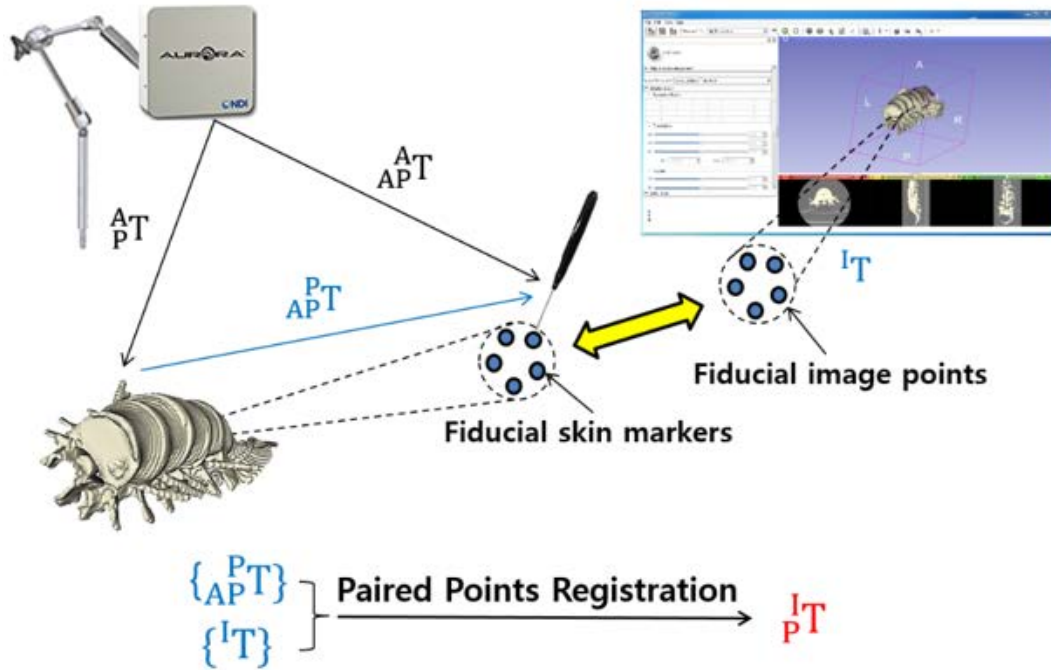
Figure 2.4 Patient-to-image registration based on the electromagnetic tracking system.

As you see in Fig 2.4, registration is performed in order to match the following two coordinate frames: 1) an image coordinate system defined by 3D Slicer and 2) a patient (real world) coordinate system defined by the electromagnetic tracking system. Fiducial points in the image coordinate system are obtained by identifying skin markers attached to the patient skin and taking the coordinates of them in the medical image set loaded in 3D Slicer. To obtain coordinates of fiducial points in the patient coordinate system, we make use of a probe tool and a reference sensor attached to the patient skin. At this time, pivot calibration is necessarily performed to determine the unknown transformation between the tracked sensor attached to the probe and the probe tip. The homogeneous transformation matrix between the field generator and the sensor attached to the probe is provided by the tracking system, being represented as follows:

$$
{}_S^A T = \begin{bmatrix} r_{00} & r_{01} & r_{02} & t_x \\ r_{10} & r_{11} & r_{12} & t_y \\ r_{20} & r_{21} & r_{22} & t_z \\ 0 & 0 & 0 & 0 \end{bmatrix}
\qquad \textbf{Equation 2.1}
$$

The position of the divot point relative to the field generator is expressed with ${}_S^A T$ and the unknown offset vector as follows:

$$\begin{bmatrix} offset_x \\ offset_y \\ offset_z \\ 1 \end{bmatrix} = \begin{bmatrix} r_{00} & r_{01} & r_{02} & t_x \\ r_{10} & r_{11} & r_{12} & t_y \\ r_{20} & r_{21} & r_{22} & t_z \\ 0 & 0 & 0 & 1 \end{bmatrix} \times \begin{bmatrix} offset_x \\ offset_y \\ offset_z \\ 1 \end{bmatrix} = \begin{bmatrix} x_0 \\ y_0 \\ z_0 \\ 1 \end{bmatrix}$$

Equation 2.2

Equation 2.2 can be re-written as follows:

$$r_{00} offset_x + r_{01} offset_y + r_{02} offset_z - 1 \cdot x_0 + 0 \cdot y_0 + 0 \cdot x_0 = -t_x$$

$$r_{10} offset_x + r_{11} offset_y + r_{12} offset_z + 0 \cdot x_0 - 1 \cdot y_0 + 0 \cdot x_0 = -t_y$$

$$r_{20} offset_x + r_{21} offset_y + r_{22} offset_z + 0 \cdot x_0 + 0 \cdot y_0 - 1 \cdot x_0 = -t_z$$

Equation 2.3

Finally, Equation 2.3 can be re-written in a matrix equation from as follows:

$$\begin{bmatrix} r_{00} & r_{01} & r_{02} & -1 & 0 & 0 \\ r_{10} & r_{11} & r_{12} & 0 & -1 & 0 \\ r_{20} & r_{21} & r_{22} & 0 & 0 & -1 \end{bmatrix} \times \begin{bmatrix} offset_x \\ offset_y \\ offset_z \\ x_0 \\ y_0 \\ z_0 \end{bmatrix} = \begin{bmatrix} -t_x \\ -t_y \\ -t_z \end{bmatrix} \qquad \text{**Equation 2.4**}$$

By sampling m measurements of a divot point with a fixed position and diverse orientations, a matrix equation is established where A is a 3m×6 rectangular matrix and B is a 3m × 1 column vector as follows:

$$A \times \begin{bmatrix} offset_x \\ offset_y \\ offset_z \\ x_0 \\ y_0 \\ z_0 \end{bmatrix} = B \qquad \text{**Equation 2.5**}$$

Here, the solution of the above system which includes the unknown variables (*offset$_x$*, *offset$_y$*, *offset$_z$*, x_0, y_0, and z_0) is derived in least-square sense in order that the residual error in a form of a root mean square error (RMSE) is minimized, being computed as follows:

$$RMSE = \sqrt{\left\| A \cdot \left[offset_x \ offset_y \ offset_z \ x_0 \ y_0 \ z_0 \right]^T - B \right\|^2 / m}$$

<div align="right">**Equation 2.6**</div>

With the obtained offset vector and the sampled data set, rotational terms can be also computed in the similar manner to that used in calculating the offset vector so that the complete homogeneous transformation matrix between the sensor and the tip is built.

With the pivot calibration result obtained by the aforementioned process, the position of the probe tool tip placed on the skin marker relative to the patient reference sensor is defined as a fiducial point in the patient coordinate system to be used for patient-to-image registration. But for a patient reference sensor, a base coordinate system of the patient fiducial points lies in the field generator of the tracking system, resulting in a crucial constraint in terms of real clinical environments that the registration result obtained using these points does not allow locational alteration of both the field generator and the patient after the registration process.
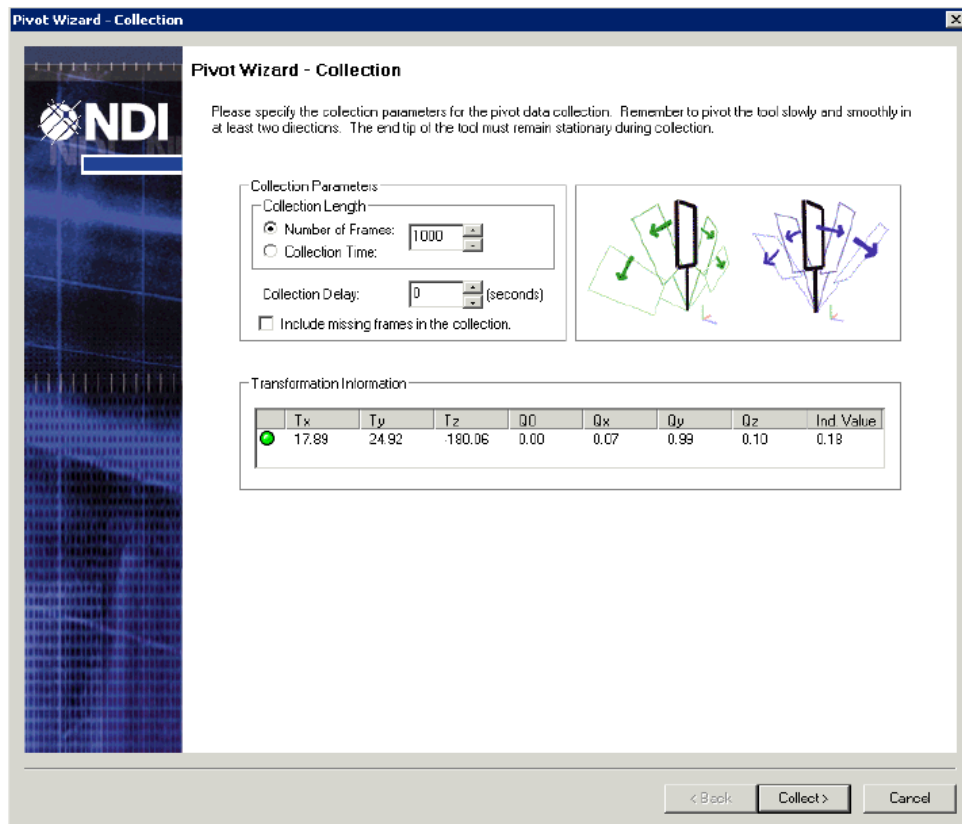
Figure 2.5 Pivot calibration of the probe tool using NDI 6D Architect software.

When we express the image fiducial points with $I = [i_1 \; i_2 \; \cdots \; i_n]^T$ and the patient fiducial points with $P = [p_1 \; p_2 \; \cdots \; p_n]^T$, a transformation matrix satisfying $I = TP$ is calculated by paired points registration (PPR) method using singular value decomposition (SVD) algorithm in order that $FRE_{Reg} = \sqrt{\frac{1}{n}\sum_{j=1}^{n}\|Tp_j - i_j\|^2}$ is minimum [18]. The cost function for calculating the transformation matrix with minimum FRE is defined with the rotational term (R) and the translational term (t) as follows:

$$f(t) = \sum_{j=1}^{n} \|Rp_j + t - i_j\|^2$$

Equation 2.7

Considering the cost function has a quadratic form, the translational term yielding the minimum FRE is determined by deriving the 1$^{\text{st}}$ order differential equation of the function and assuming it to be zero as follows:

$$\frac{\partial f(t)}{\partial t} = 2\sum_{j=1}^{n}(Rp_j + t - i_j)$$

$$= 2t\sum_{j=1}^{n}(1) + 2R\sum_{j=1}^{n}(p_j) - 2\sum_{j=1}^{n}(i_j) = 0$$

Equation 2.8

Rearranging the above equation, we obtain t which is expressed with centers of mass of the two point sets as follows:

$$t = \frac{1}{n}\sum_{j=1}^{n}(i_j) - R\frac{1}{n}\sum_{j=1}^{n}(p_j)$$

$$= \bar{i} - R\bar{p}$$

Equation 2.9

Substituting the calculated t in Equation 2.9 into Equation 2.7 to find the unknown rotation matrix (R) we get an equation for the cost function with respect to R as follows:

$$f(R) = \sum_{j=1}^{n} \left\| Rp_j + \bar{i} - R\bar{p} - i_j \right\|^2$$

$$= \sum_{j=1}^{n} \left\| R(p_j - \bar{p}) - (i_j - \bar{i}) \right\|^2$$

$$= \sum_{j=1}^{n} \left\| Rx_j - y_j \right\|^2$$

Equation 2.10

where $x_j = p_j - \bar{p}$ and $y_j = i_j - \bar{i}$.

To get the minimum value of $f(R)$, we should try to minimize $\left\| Rx_j - y_j \right\|^2$. Expanding it gives the following

result as shown below:

$$\left\| Rx_j - y_j \right\|^2 = \left(Rx_j - y_j\right)^T \left(Rx_j - y_j\right)$$

$$= (x_j^T R^T - y_j^T)(Rx_j - y_j)$$

$$= x_j^T x_j - x_j^T R^T y_j - y_j^T Rx_j + y_j^T y_j$$

$$= x_j^T x_j - 2y_j^T Rx_j + y_j^T y_j$$

Equation 2.11

where we can consider $x_j^T R^T y_j = (x_j^T R^T y_j)^T = y_j^T Rx_j$ since $x_j^T R^T y_j$ is a scalar term.

From Equation 2.11, we know that $f(R)$ will be minimum in case that $y_j^T Rx_j$ term is maximum. Assuming

that X is a 3-by-n matrix which has x_j as a column vector and Y is a 3-by-n matrix which has y_j as a column

vector, we can consider the following:

$$\sum_{j=1}^{n} (y_j^T Rx_j) = tr(Y^T RX)$$

Equation 2.12

We can use the property of trace to give an equation as follows:

$$tr(Y^T RX) = tr(RXY^T)$$

<div align="right">**Equation 2.13**</div>

Supposing that XY^T is a single matrix and performing SVD on the matrix, the above equation can be modified as follows:

$$tr(RXY^T) = tr(RU\Sigma V^T)$$
$$= tr(\Sigma V^T RU)$$

<div align="right">**Equation 2.14**</div>

When we think of $V^T RU$ as another single matrix, it is an orthonormal matrix in that both V and U are an orthonormal matrix which is derived from SVD, and R is also a rotation matrix. The trace of $\Sigma V^T RU$ can be maximized, which generates the minimum value of $f(R)$, in case that $V^T RU$ is an identity matrix. It is because the value of matrix components in $V^T RU$ is no more than one, which is a property of an orthonormal matrix. Considering that, we can get the rotation matrix, R as follows:

$$V^T RU = I$$
$$R = VU^T$$

<div align="right">**Equation 2.15**</div>

At this moment, we should check if the calculated R matrix represents rotation or reflection; The determinant of R is either +1 for rotation or -1 for reflection. In case that the derived R is a reflection matrix, the matrix can be modified in order that it represents rotation by the following simple procedure:

$$R = V \begin{bmatrix} 1 & 0 & 0 \\ 0 & 1 & 0 \\ 0 & 0 & det(VU^T) \end{bmatrix} U^T$$

<div align="right">**Equation 2.16**</div>

Substituting the derived R into Equation 2.9, we can get the translation vector t which completely builds the 4-by-4 patient-to-image registration matrix together with the rotation matrix R as follows:

$$T = \left[\begin{array}{c|c} R & t \\ 0_3{}^T & 1 \end{array} \right]$$

<div align="right">**Equation 2.17**</div>

With the computed patient-to-image registration matrix ($_P^I T$), the tracking utility calculates the final transformation matrix representing the pose of the surgical tool with respect to the patient anatomy on the medical image set by some simple matrix algebra in real time as follows:

$$_{AP}^{I}T = {_P^I}T \ {_P^A}T^{-1} {_{AP}^A}T \qquad\qquad \textbf{Equation 2.18}$$

The pose information is transmitted via socket communication and visualized in 3D virtual space of our visualization platform, 3D Slicer, as shown on Fig 2.6.
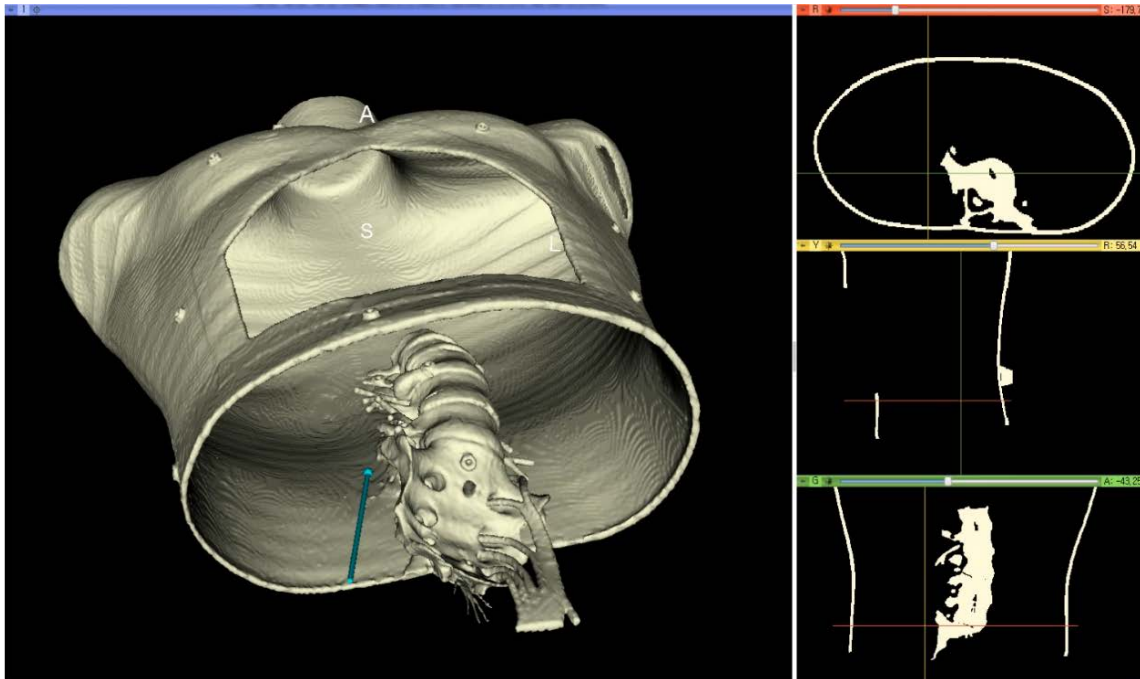
Figure 2.6 3D view and MPR image-based 2D navigation view of the phantom navigation.

2.3 Hybrid Navigation System

As described in the previous chapters, In performing surgical navigation to assist the ELND procedure where a flexible catheter is inserted inside the patient body, we have no choice but to adopt the EMTS as our tracking modality rather than the OTS due to its line-of-sight limitation. However, the EMTS-based surgical navigation suffers from the chronic inaccuracy problem in the EMTS, the tracking accuracy of which is at one order of magnitude lower level in comparison with that of the OTS. In this regard, we propose a new surgical navigation system for the EDS procedure, which makes use of the EMTS and the OTS in a complementary way to compensate for low tracking accuracy of the EMTS and consequently obtain higher navigation accuracy compared with that of the EMTS-alone navigation system. Our navigation system aims to both provide 3D visual information with reliable accuracy for surgeons easily understanding the surgical situation and replace fluoroscopy to overcome postoperative side effects resulting from exposure to high radiation doses and possible contrast agent-induced adverse reactions. Figure shows the conceptual diagram of the proposed system. For the setup of the proposed system, we used a commercially available OTS (Polaris Vicra, NDI, Waterloo, Canada) with the aforementioned EMTS. The red arrow represents an intraoperative procedure to be performed in the operating room. The black arrow indicates relationships between each tracking system and tools tracked by it: a surgical tool (catheter) is tracked by the EMTS, a patient reference marker tracked by the OTS, and a calibration probe tool tracked by the both tracking systems. Finally, the blue one shows data flows into the navigation workstation.
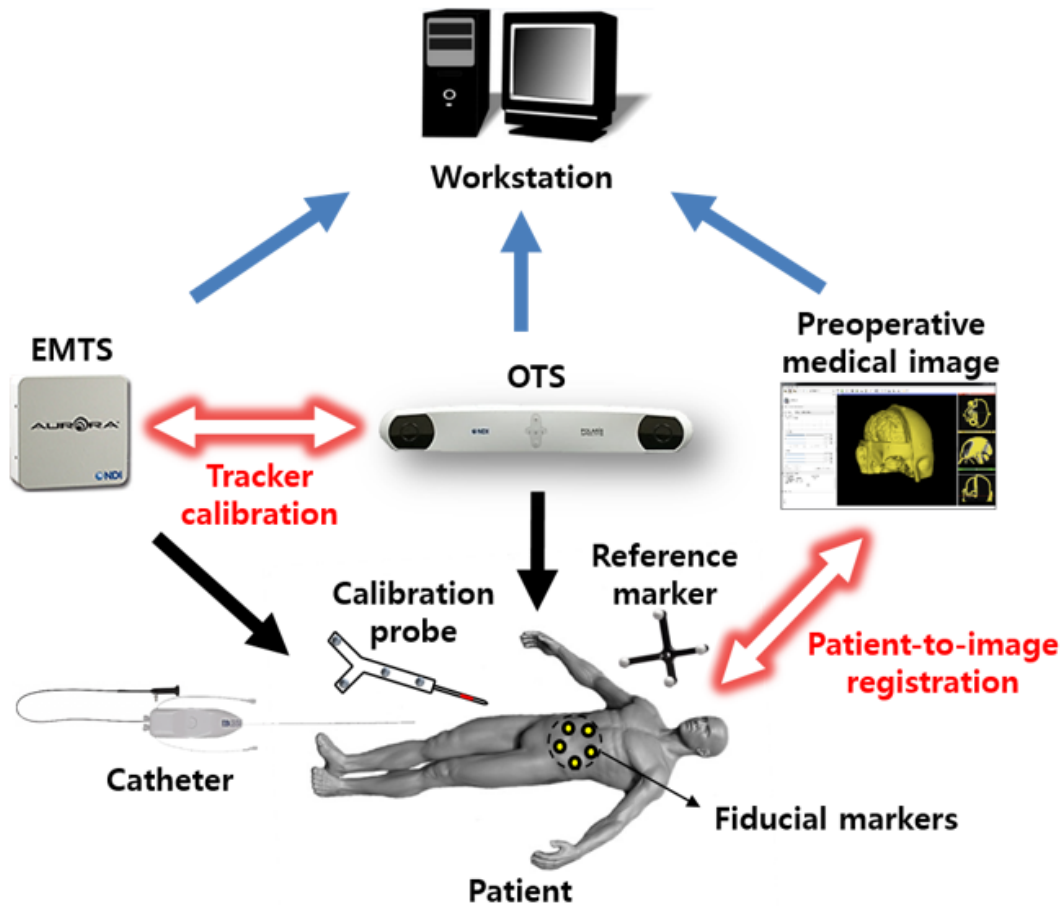
Figure 2.7 Configuration of hybrid navigation system.

The followings will describe crucial points on (1) combining an EMTS and an OTS into a hybrid navigation system: how to make a calibration tool which enables the cumbersome calibration process to be conducted easily and conveniently and how to effectively calibrate two different tracking modalities, (2) conducting patient-to-image registration using an OTS instead of an EMTS and applying that result to the EMTS-based pose data of the surgical tool for the purpose of obtaining better navigation accuracy.

2.3.1 Tracker Calibration between Tracking Systems

Tracker calibration is a process for calculating the positional relationship between the EMTS and the OTS. First, an optical marker frame is attached to the field generator of the EMTS, which enables the EMTS to be tracked in real time by the OTS. After that, we need to know the transformation between the field generator and the optical marker frame attached to it so that coordinate conversion between the EMTS and the OTS is able to

be performed. To be specific, two different point sets are acquired to register the following coordinate systems: the FG coordinate system and the optical marker coordinate system. They are available from measurements in both tracking systems directly or with simple matrix multiplication as follows:

$$_{EP}^{E}T \quad \text{providing } \boldsymbol{E} = [e_1 \; e_2 \; \cdots \; e_n]^T \text{ for FG}$$

$$_{OP}^{EM}T = {}_{EM}^{O}T^{-1} {}_{OP}^{O}T \quad \text{providing } \boldsymbol{EM} = [em_1 \; em_2 \; \cdots \; em_n]^T \text{ for optical marker}$$

In common with the case of patient-to-image registration, tracker calibration can be performed without the optical marker attached to the field generator. However, the calibration result would be useless if either of the two tracking systems changes its location, which could be a tremendous constraint in applying the system in complicated clinical environments.

With the above point sets, a homogeneous transformation matrix $({}_{E}^{EM}T)$ satisfying $EM = TE$, which represents the pose relationship between the optical marker frame and the field generator, is calculated by PPR method in order that $FRE_{Cal} = \sqrt{\frac{1}{n}\sum_{1}^{n}\|Te_j - em_j\|^2}$ is minimum.
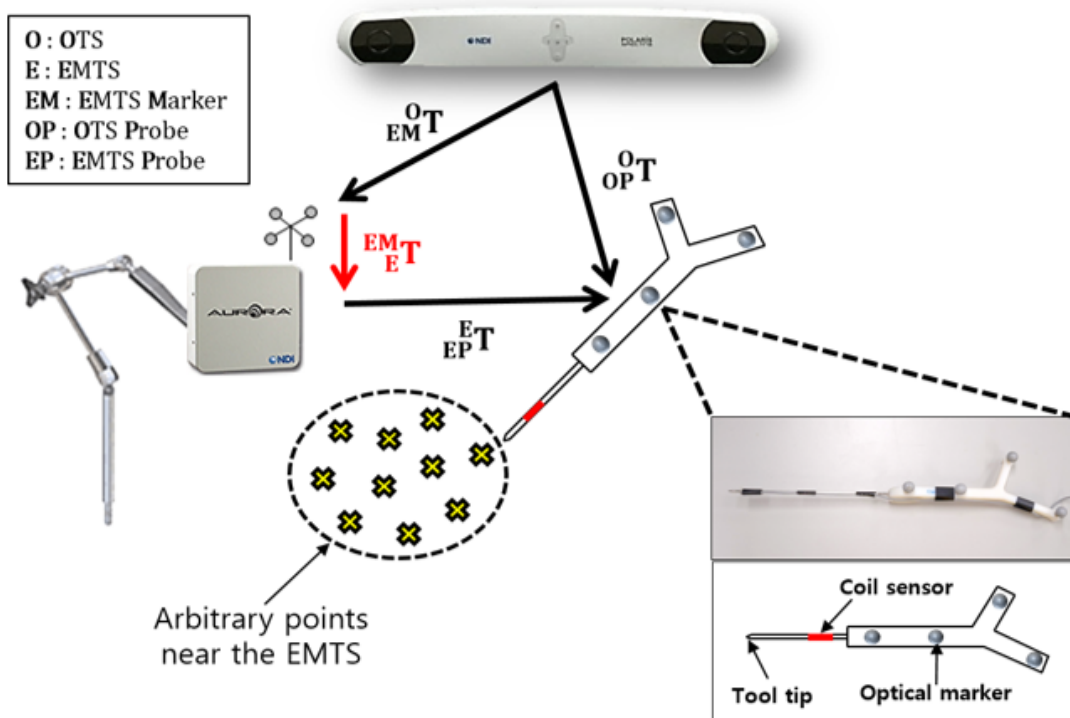
Figure 2.8 Tracker calibration between the OTS and the EMTS.

Once we know the relationship via tracker calibration, which is not going to be changed during the surgical procedure, the pose of the catheter-type magnetic sensor can be reported in the OTS coordinate frame in real time and the patient-to-image registration matrix with high accuracy which is obtained by using the OTS can be applied in our navigation system, thus yielding better navigation accuracy. Moreover, unless the location of the optical marker set attached to the field generator is altered, the result of tracker calibration is independent of locational change of the tracking systems in the operating room since the EMTS is tracked by the OTS in real time.

For the purpose of avoiding time delay and facilitating the tracker calibration process during the real procedure, we designed a calibration probe which enables measurements obtained by using the probe to be reported in both coordinate systems of the EMTS and the OTS at the same time. Figure depicts our calibration probe, the main frame of which is manufactured by rapid prototyping machine. In the probe, an optical marker set and a magnetic coil sensor are integrated in a single body and the tracked positions of the optical marker and the coil sensor by each tracking system are aligned to be the tool tip of the probe via pivot calibration process mentioned in the previous chapter. Use of our calibration probe offers two definite advantages in terms of real operating environments: we don't need to acquire a fiducial point set, which is used for tracker calibration, twice for each tracking system. According to our experiments, the intraoperative calibration time is reduced by 60 % compared with that taken in case of no use of the calibration probe. In addition, there is no need for a calibration object, or phantom which is specially designed for use in tracker calibration; locating the probe in several random points near the field generator is enough to acquire fiducial points for the both tracking system, which provides convenience to surgeons. Actually, this probe is utilized for patient-image registration as well as tracker calibration.
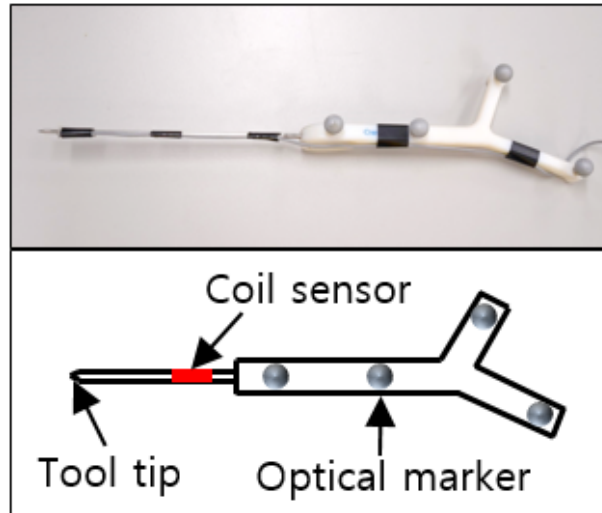
Figure 2.9 Calibration probe designed to perform tracker calibration fast and conveniently.

2.3.2 Patient-to-Image Registration

Patient-to-image registration is the most important procedure in performing surgical navigation in that accuracy of the registration result directly influences that of surgical navigation. Most of basic procedures and related mathematics for hybrid navigation system identically follow those of registration in EMTS-based surgical navigation which are delineated in the previous chapter. In hybrid navigation setup, patient-to-image registration is conducted by using the OTS rather than the EMTS, considering that the tracking data from the EMTS has a higher degree of inaccuracy than that from the OTS, which is used as fiducial points for registration to cause an inaccurate registration result. Figure depicts configuration of patient-to-image registration using OTS. In hybrid navigation setup, patient-to-image registration is performed in order to match the following two coordinate systems: 1) an image coordinate system defined by 3D Slicer and 2) a patient (real world) coordinate system defined by the optical tracking system, not the electromagnetic tracking system. Fiducial points in the image coordinate system are obtained from the medical image set loaded in 3D Slicer. Patient fiducial points are acquired by using an optical probe tool (calibration probe) and an optical reference marker attached to the patient skin: The position of the probe tool tip placed on the skin marker relative to the patient reference marker is defined as a fiducial point in the patient coordinate system to be used for patient-to-image registration. Each fiducial point set is available respectively from 3D Slicer and measurements in the OTS with simple matrix multiplication as follows:

$$^IT \quad \text{providing } I = [i_1 \ i_2 \ \cdots \ i_n]^T \text{ for image}$$

$$^{PM}_{OP}T = {}^{O}_{PM}T^{-1} \, {}^{O}_{OP}T \quad \text{providing } PM = [pm_1 \ pm_2 \ \cdots \ pm_n]^T \text{ for optical marker}$$

In common with the case of EMTS-based navigation system, a homogeneous transformation matrix satisfying $I=TPM$ is calculated by PPR method in order that $FRE_{Reg} = \sqrt{\frac{1}{n}\sum_{j=1}^{n}\|Tpm_j - i_j\|^2}$ is minimum.
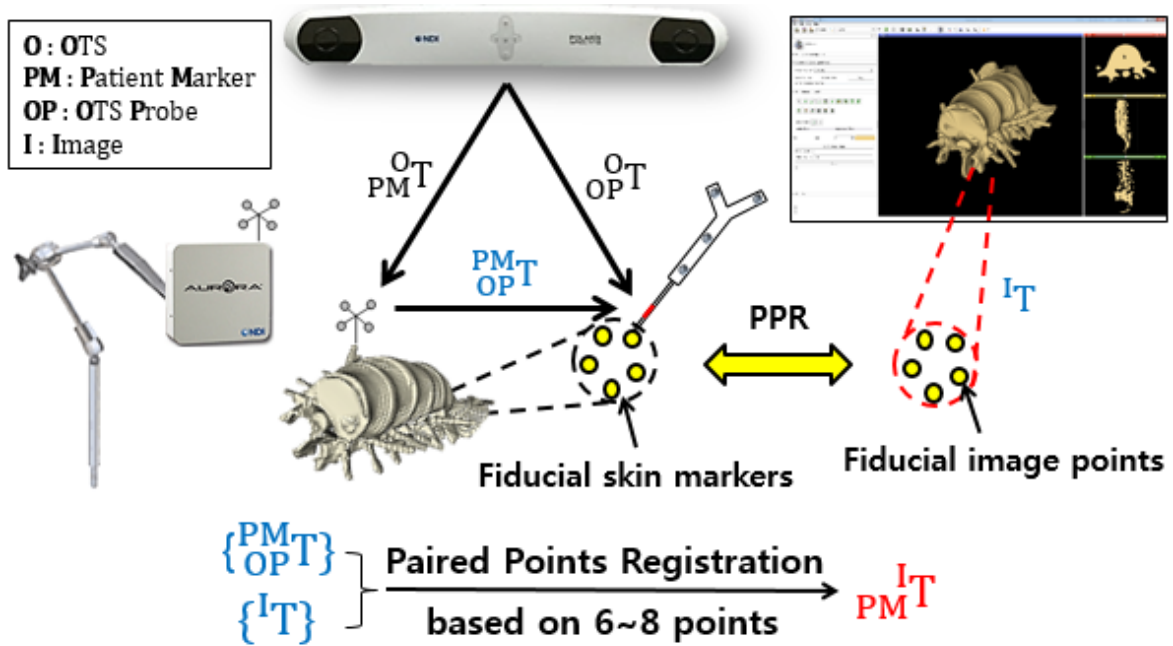
Figure 2.10 Patient-to-image registration using the optical tracking system.

At this point, the registration matrix is computed with a basis on tracking data from the OTS, which means the registration accuracy is highly reliable due to high accuracy of the OTS, compared with that of EMTS-based registration. After registration is done, the pose data of a surgical tool (catheter) from the EMTS is transformed into the coordinate frame of the OTS patient marker using the tracker calibration result $\left(^{EM}_{E}T\right)$ as follows:

$$^{PM}_{C}T = {}^{O}_{PM}T^{-1} \, {}^{O}_{EM}T \, {}^{EM}_{E}T \, {}^{E}_{C}T$$

Equation 2.19

Finally, the intermediate pose data ($^{PM}_{C}T$) is transformed into the image coordinate frame with the computed OTS-based registration matrix ($_{PM}^{I}T$) as follows:

$$^{I}_{C}T = {}_{PM}^{I}T \; {}^{PM}_{C}T$$

Equation 2.20

The final pose data ($^{I}_{C}T$), which is a pose relationship between the catheter and the patient anatomy identified in the medical images, is transmitted to 3D Slicer via socket communication and then can be visualized with reliable accuracy on the medical images in real time.

2.4 Compensation of Error from Electromagnetic Field Distortion

The presence of nearby metallic structures or electronic devices negatively affects the accuracy of the tracking data from an EMTS [15]. In many cases, it is not allowed either to take such error-causing object out of the tracking volume or to reposition the FG. A surgical table, surgical bed, monitors, surgical instruments or a C-arm device are typical examples of a distortion-causing object which could not be put aside in the operating room. In addition, the measurement error of an EMTS increases proportionally to the fourth power of the distance between the FG and the tracked sensor as previously mentioned. In case that it is not possible to position the FG close to the tracked sensor, or the patient due to complicated surgical environments, a higher degree of the tracking error could take place, degrading the overall navigation accuracy. In the previous chapter, the hybrid navigation system was suggested to address the navigation inaccuracy of EMTS-based navigation system by making use of an OTS and an EMTS in a complementary way. Even though registration accuracies are improved with use of an OTS in the hybrid navigation setup, inherent tracking error of an EMTS still degrades the accurate registration result obtained by using an OTS. In this chapter, for further improvement in navigation accuracy, we consider integration of compensation of the tracking error of an EMTS stemming from electromagnetic field distortion into our hybrid navigation system.
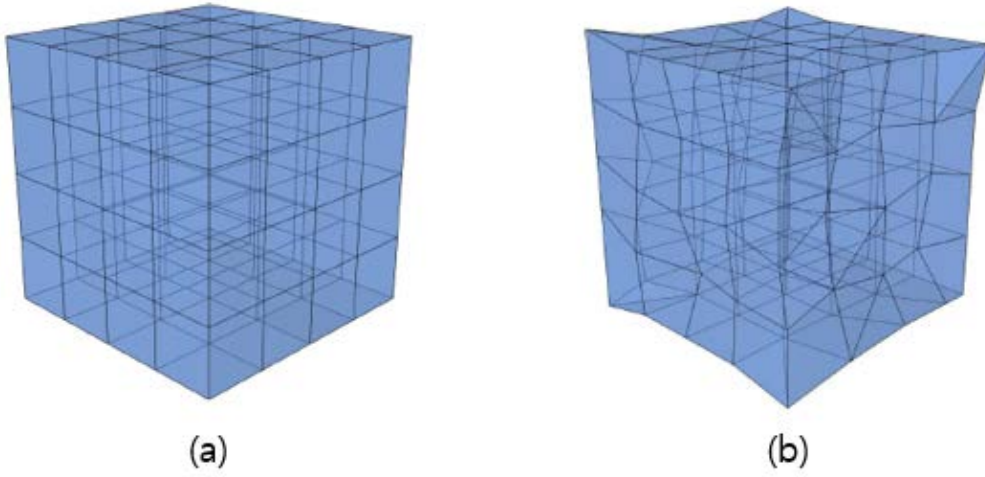
Figure 2.11 (a) Pure electromagnetic field and (b) distorted electromagnetic field.

2.4.1 Definition of Error

There exist both the position error and the orientation error in an EMTS. However, in case of ELND procedures, the orientation of a surgical tool (catheter) is redundant information in that grasping the position of the catheter located inside the patient body is enough to understand the current surgical situation. In this regard, we determined to deal with the position error without addressing the orientation error.

Assuming that measured (distorted) position from an EMTS and reference position from an OTS are respectively expressed in a vector form as follows:

$$\vec{p}_{measured} = [x_{measured}, y_{measured}, z_{measured}]^T$$

$$\vec{p}_{reference} = [x_{reference}, y_{reference}, z_{reference}]^T$$

Equation 2.21

position error is defined as follows:

$$\vec{e} = \vec{p}_{reference} - \vec{p}_{measured}$$

$$\begin{pmatrix} e_x \\ e_y \\ e_z \end{pmatrix} = \begin{pmatrix} x_{reference} \\ y_{reference} \\ z_{reference} \end{pmatrix} - \begin{pmatrix} x_{measured} \\ y_{measured} \\ z_{measured} \end{pmatrix}$$

Equation 2.22

2.4.2 Data Acquisition

To compensate the distorted measurements from an EMTS, an additional data acquisition procedure is necessary. This is usually accomplished by using a secondary tracking device or measurement tool providing a ground truth data with reliable accuracy. In various error correction techniques, it is a common procedure to record a set of distorted measurements from an EMTS and the corresponding undistorted reference measurements with an additional tracking system or measurement tool (in our case, an OTS). In medical environments, this is usually done in the operating room before starting a clinical procedure. At this time, it is important to keep the setup unchanged during the whole procedure. If the field generator or distortion-causing objects are repositioned, the measurements reflecting the error field in the altered environment must be reacquired.

There are many ways where data can be collected, which should be properly selected depending on a particular application. They can be categorized in terms of two perspectives: 1) dynamic and static collection, and 2) Robotic and manual collection. Dynamic method allows data from the both tracking systems to be collected at the same time while a calibration probe is moved through the tracking volume without stopping to acquire the measurements. Dynamic method enables a great deal of data to be collected for a short time, but it suffers two main problems: 1) degraded tracking accuracy for moving targets inherent to tracking systems and 2) uneven distribution of data in case of the manual collection. In case of the static method, two sets of measurements from each tracking system are separately acquired with stability. However, it takes a longer time to collect data more than two times than the dynamic method, and possibly requires a special calibration object, or grid. In our case, a compromise approach would be appropriate in terms of clinical applications: 1) place the probe in a given position, 2) acquire the measurement data from the both tracking system, and 3) move the probe to the next position. Robotic collection is ideal for collecting a large number of data points with a predefined data interval based on the above mentioned compromise method. However, it requires a robotic system for data collection, which is not practical for use in clinical environments. In our case, we only have to collect data using the compromise method with our calibration probe which is designed for tracker calibration. Based on the measurement data from the OTS, The ground truth data is obtained by applying the result of tracker calibration between the EMTS and the OTS which is conducted for the hybrid navigation setup prior to data collection.

2.4.3 Error Modeling

Assuming that the location of the FG remains unchanged and the surrounding metallic structures do not move, the static error is modeled as a function of the position of the sensor. Interpolation techniques based on a uniformly spaced lookup table (LUT) could be applied for compensating the error. However, these techniques are based on the assumption that the distortion field is linear within a given subspace, which is not always the case. In addition, a lot of precise and regularly spaced measurements need to be acquired. In this regard, we adopted a fitting-based correction technique which generally performs better than interpolation-based ones in that the fit can take a form of a high-order polynomial that may very well capture the shape of the distorted magnetic field, and fewer measurements may be needed [19]. With the collected measurement data, we can build position correction equations using high-order polynomials as follows [20]:

$$\vec{p}_{reference} = \vec{p}_{measured} + \sum_{j=1}^{m} \begin{pmatrix} c_{xj} \\ c_{yj} \\ c_{zj} \end{pmatrix} x^{p_j'} \, y^{p_j''} \, z^{p_j'''}$$

$$\overrightarrow{e'} = \begin{pmatrix} e_x' \\ e_y' \\ e_z' \end{pmatrix} = \sum_{j=1}^{m} \begin{pmatrix} c_{xj} \\ c_{yj} \\ c_{zj} \end{pmatrix} x^{p_j'} \, y^{p_j''} \, z^{p_j'''}$$

Equation 2.23

where $c_{xj}, c_{yj},$ and c_{zj} are the polynomial coefficients, m is the number of terms in the polynomial that depends on the order r of the polynomial given by $m = \frac{(r+1)(r+2)(r+3)}{6}$, and p_j', p_j'', and p_j''' are the nonnegative integer powers which are determined in order that all permutations of $\{p_j', p_j'', p_j'''\}$ are unique and $0 \leq p_j' + p_j'' + p_j''' \leq r$. $x^{p_j'} \, y^{p_j''} \, z^{p_j'''}$ adopted as the basis function of the polynomial is able to be modified to different forms of functions, depending on users' need. We must calculate $c_{xj}, c_{yj},$ and c_{zj} such that the fitting polynomials closely approximate the position error $\overrightarrow{e'}$. With n measurements, they can be found by minimizing the following function:

$$f = \sum_{i=1}^{n} \left\| \overrightarrow{e_i} - \overrightarrow{e_i'} \right\|^2$$

Equation 2.24

which is a well-known least-square fit problem.

There are two ways for obtaining the solution. The first one is the algebraic method based on the matrix computation. With n measurements, we can build the following simultaneous equations for x coordinate:

$$\begin{cases} c_{x1}x_1^{p_1}\,y_1^{p_1}\,z_1^{p_1} & + \cdots + c_{xj}x_1^{p_j}\,y_1^{p_j}\,z_1^{p_j} & + \cdots + c_{xm}x_1^{p_m}y_1^{p_m}\,z_1^{p_m} & = e_{x1} \\ & \vdots & \\ c_{x1}x_i^{p_1}\,y_i^{p_1}\,z_i^{p_1} & + \cdots + c_{xj}x_i^{p_j}\,y_i^{p_j}\,z_i^{p_j} & + \cdots + c_{xm}x_i^{p_m}y_i^{p_m}\,z_i^{p_m} & = e_{xi} \\ & \vdots & \\ c_{x1}x_n^{p_1}\,y_n^{p_1}\,z_n^{p_1} & + \cdots + c_{xj}x_n^{p_j}\,y_n^{p_j}\,z_n^{p_j} & + \cdots + c_{xm}x_n^{p_m}y_n^{p_m}\,z_n^{p_m} & = e_{xn} \end{cases}$$

Equation 2.25

which can be converted into the following matrix equation:

$$\begin{pmatrix} a_{1,1} & \cdots & a_{1,j} & \cdots & a_{1,m} \\ \vdots & \vdots & \vdots & \vdots & \vdots \\ a_{i,1} & \cdots & a_{i,j} & \cdots & a_{i,m} \\ \vdots & \vdots & \vdots & \vdots & \vdots \\ a_{n,1} & \cdots & a_{n,j} & \cdots & a_{n,m} \end{pmatrix} \begin{pmatrix} t_1 \\ \vdots \\ t_j \\ \vdots \\ t_m \end{pmatrix} = \begin{pmatrix} b_1 \\ \vdots \\ b_i \\ \vdots \\ b_n \end{pmatrix}$$

$$\boldsymbol{At = b}$$

Equation 2.26

where $a_{i,j} = x_i^{p_j}\,y_i^{p_j}\,z_i^{p_j}$, $t_j = c_{xj}$, $b_i = e_{xi}$, $\boldsymbol{A}$ is a n-by-m matrix, $\boldsymbol{t}$ is a m-by-1 vector which is the solution, and $\boldsymbol{b}$ is a n-by-1 vector. The above equation can be solved in least-square sense by applying the pseudo inverse method as follows:

$$\boldsymbol{t} = pinv(\boldsymbol{A})\boldsymbol{b}$$
$$= (\boldsymbol{A}^T\boldsymbol{A})^{-1}\boldsymbol{A}^T\boldsymbol{b}$$

Equation 2.27

If we try to check if the derived t is the solution which causes the square of the residual sum to be minimum, we can consider a problem of finding the minimum of $\|b - At\|^2$. Partially differentiating $\|b - At\|^2$ with respect to t and letting it be zero to acquire the minimum t which makes the above quadratic function minimum, we get the following result:

$$-2A^T(b - At) = 0$$

$$t = (A^T A)^{-1} A^T b$$

<div align="right">**Equation 2.28**</div>

which is the same result as that in Equation 2.27.

Actually, when it comes to solving $At = b$ in Equation 2.26, the pseudo inverse method described in Equation 2.27 is often replaced by SVD or QR factorization technique for the purpose of improving the accuracy of the solution.

The other method for obtaining the solution is the analytic method. Partial differentiation of $\|b - At\|^2$ with respect to each unknown polynomial coefficient gives rise to the following m equations:

$$\begin{cases} \sum_{j=1}^{m} t_j \sum_{i=1}^{n} a_{i,j} a_{i,1} = \sum_{i=1}^{n} b_i a_{i,1} \\ \vdots \\ \sum_{j=1}^{m} t_j \sum_{i=1}^{n} a_{i,j} a_{i,k} = \sum_{i=1}^{n} b_i a_{i,k} \\ \vdots \\ \sum_{j=1}^{m} t_j \sum_{i=1}^{n} a_{i,j} a_{i,m} = \sum_{i=1}^{n} b_i a_{i,m} \end{cases}$$

<div align="right">**Equation 2.29**</div>

where $= 1, \ldots, n$. We can achieve the solution by computing these m simultaneous equations. The polynomial coefficients for y and z coordinates can be also computed in the same way mentioned above.

2.4.4 Real-time Measurement Compensation

Once we obtain the polynomial coefficients of the error model, it is possible to compute the corrected value for the distorted measurements from an EMTS in real time as follows:

$$\vec{p}_{corrected} = \vec{p}_{measured} + \overrightarrow{e\,'}$$

$$\begin{pmatrix} x_{corrected} \\ y_{corrected} \\ z_{corrected} \end{pmatrix} = \begin{pmatrix} x_{measured} \\ y_{measured} \\ z_{measured} \end{pmatrix} + \sum_{j=1}^{m} \begin{pmatrix} c_{xj} \\ c_{yj} \\ c_{zj} \end{pmatrix} x^{p_j{'}} \ y^{p_j{''}} \ z^{p_j{'''}}$$

Equation 2.30

After that, the corrected position vector is applied to the transformation matrix representing the catheter pose in the coordinate system of the EMTS as follows:

$$_{C}^{E}T = \begin{bmatrix} r_{00} & r_{01} & r_{02} & t_x \\ r_{10} & r_{11} & r_{12} & t_y \\ r_{20} & r_{21} & r_{22} & t_z \\ 0 & 0 & 0 & 0 \end{bmatrix}$$

$$_{C}^{E}T_{corrected} = \begin{bmatrix} r_{00} & r_{01} & r_{02} & x_{corrected} \\ r_{10} & r_{11} & r_{12} & y_{corrected} \\ r_{20} & r_{21} & r_{22} & z_{corrected} \\ 0 & 0 & 0 & 0 \end{bmatrix}$$

Equation 2.31

In turn, the corrected pose of the catheter ($_{C}^{E}T_{corrected}$) is applied to the final matrix transmitted to 3D Slicer as follows:

$$_{C}^{PM}T = {_{PM}^{O}T}^{-1} \, _{EM}^{O}T \, _{E}^{EM}T \, _{C}^{E}T$$

$$_{C}^{PM}T_{corrected} = {_{PM}^{O}T}^{-1} \, _{EM}^{O}T \, _{E}^{EM}T \, _{C}^{E}T_{corrected}$$

Equation 2.32

Finally, the error-compensated pose data of the catheter is visualized in the medical images in 3D Slicer as follows:

$$_C^I T_{corrected} = \,_{PM}^I T \,_C^{PM} T_{corrected}$$

<div align="right">**Equation 2.33**</div>

2.5 Development of Navigation Software

We developed a navigation software which can be utilized in performing surgical navigation for assisting catheter insertion procedures. In this section, we will introduce each sub-functionality in our navigation software and implementation pipeline.

2.5.1 Functionality

Tracking Client

Tracking client was designed to be used for both the optical tracking system and the electromagnetic system. Tracking data consist of a 3DOF position vector and quaternion values which can be transformed into a rotation matrix or Euler's angle. The tracking information is transmitted from the main system to the navigation software by RS-232C communication and the transmission rate can be adjusted by controlling the baud rate. To track pose of user-customized tools, tracking systems need to know their own geometry. For that, tool definition files called ROM are loaded in the tracking utility; ROM is a file which gives information of a tool geometry to be tracked. The maximum number of tools to be tracked simultaneously by each tracking system is four. The estimation of how well the system calculated the tracking value is provided with a unit less value scaled to fall between 0 and 9.9 where 0 indicates the absence of error and 9.9 is the highest indication of error. Indicator value less than 1.0 are typically considered acceptable and users should set their own thresholds when acquiring tracking data which is used for registration to affect the registration accuracy. In addition, the status of each tool is provided with both text and color display, indicating whether the tool is inside the tracking volume or missing. Especially, intuitive display of red color in case of missing facilitates acquisition of tracking data.
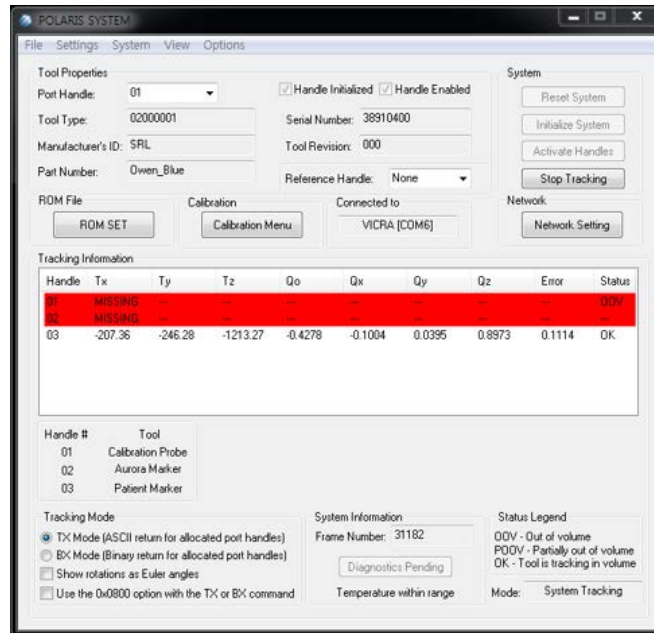
Figure 2.12 Tracking Client

Registration Client

Registration client performs patient-to-image registration to calculate the resultant transformation matrix and the registration accuracy and is integrated in a module of the navigation software. Our registration utility is a modified version of the one developed by Hong et al. [21]. Two point sets are loaded from dat or txt file. The format of the loaded file also allows annotation comma separated value (acsv) which is a data format generated from 3D Slicer. The maximum number of fiducial points is set to ten, but that number is able to be adjusted by simple modification of the software. Registration error in each fiducial point is provided in a form of both a numerical value and intuitive color display: red for the biggest error and green for the smallest error. Boundary error value determining the color can be adjusted depending on the required accuracy in each surgical procedure. When the registration error is quite big, the relevant fiducial point pairs which cause the error can be excluded by referring to the color display and registration can be re-conducted to generate better registration result. The calculated registration matrix is saved as a dat or a txt file format and loaded in the navigation utility.
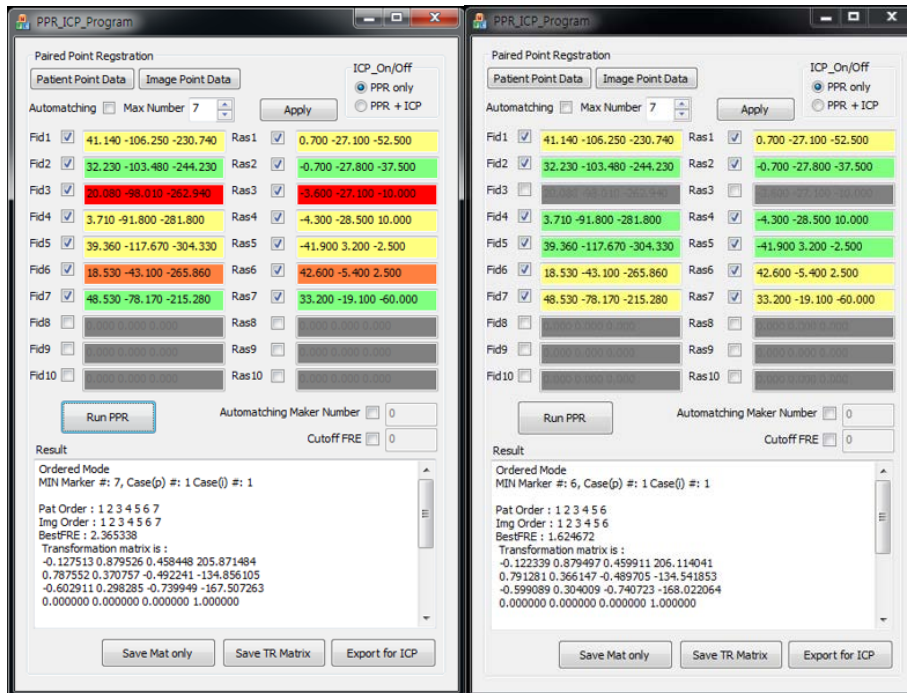
Figure 2.13 Registration client. Registration result with large error (left) and registration result improved by leaving out a pair of outliers among fiducial points (right).

Navigation Client

Navigation client includes diverse functionalities required to perform surgical navigation. First, it provides socket communication between the tracking client and the visualization platform, 3D Slicer. Sharing the tracking information between the EMTS tracking client and the OTS tracking client is available for convenient acquisition of measurement data used for tracker calibration. Registration client, pivot calibration software, and 3D Slicer are able to be executed by the button interface in the navigation client. Registration matrix can be either loaded from the prepared result file or set to identity matrix, depending on user needs. Performing patient-to-image registration or surgical navigation with and without a patient reference sensor simultaneously is considered just in case that registration result calculated using the reference sensor could be useless when the reference sensor is broken or detached from the original location after the registration. Acquisition of patient fiducial points is easily conducted by the data collection interface in the navigation client. In addition, the pose data of the surgical tool during the procedure can be recorded with a time tag in a log file.
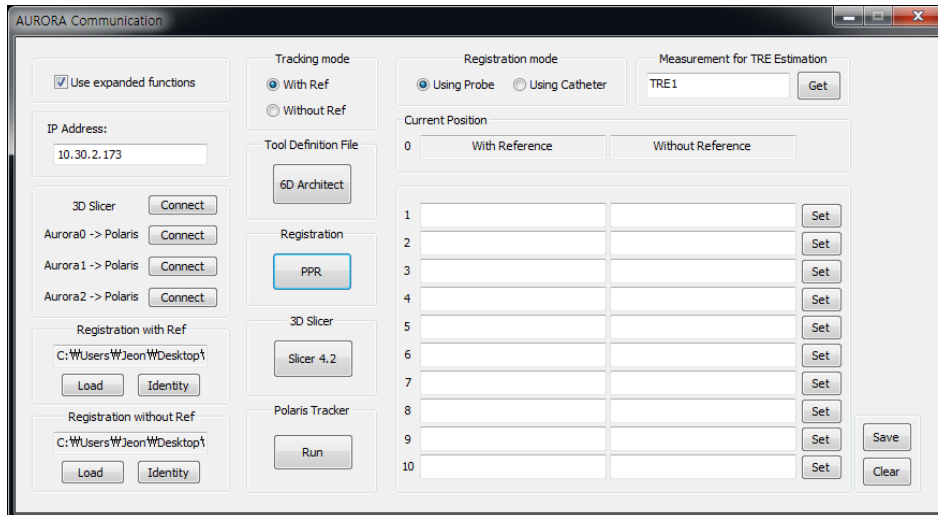
Figure 2.14 Navigation client for EMTS.
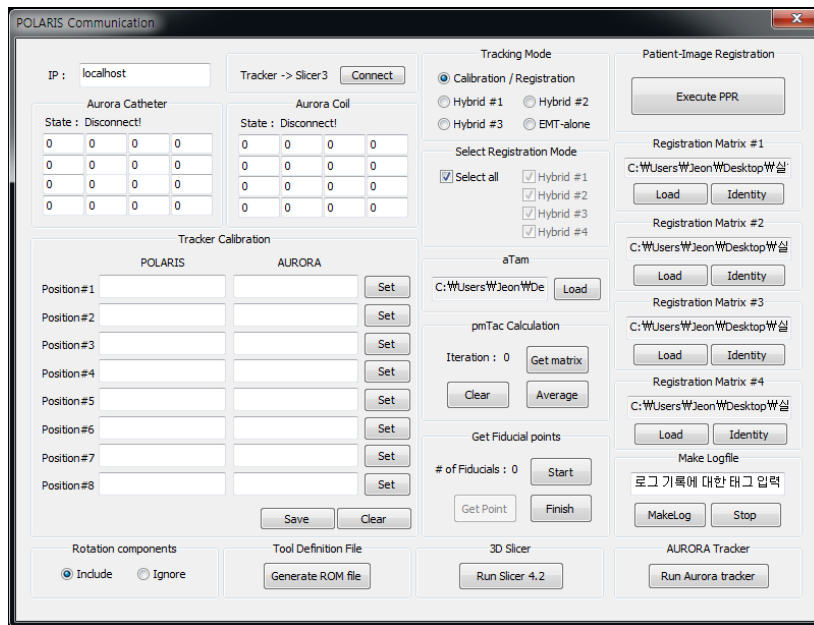
Figure 2.15 Navigation client for OTS.

Error Modeling Client

Error modeling client simultaneously collects the tracking data from the tracking clients of both EMTS and OTS. The collected data is used for estimating the initial error and performing polynomial fitting, or saved as a txt file for future uses. At this time, we can selectively exclude the acquired pose data in case that the data could be an outlier which causes the error model to be inaccurate. The calculated model parameters can be saved and

loaded in the navigation client to perform real-time compensation for the tracking error. Right after polynomial fitting, we can estimate how well the derived error model reflects the actual error by calculating root mean square error (RMSE) for the compensated pose data.

Figure 2.16 Software for collecting measurement data from the OTS and the EMTS and calculating the parameters of the error model

2.5.2 Implementation Procedure

Implementation procedure for compensation of error field is provided as shown on Fig 2.17.

Figure 2.17 Flow diagram showing compensation for tracking error in EMTS.
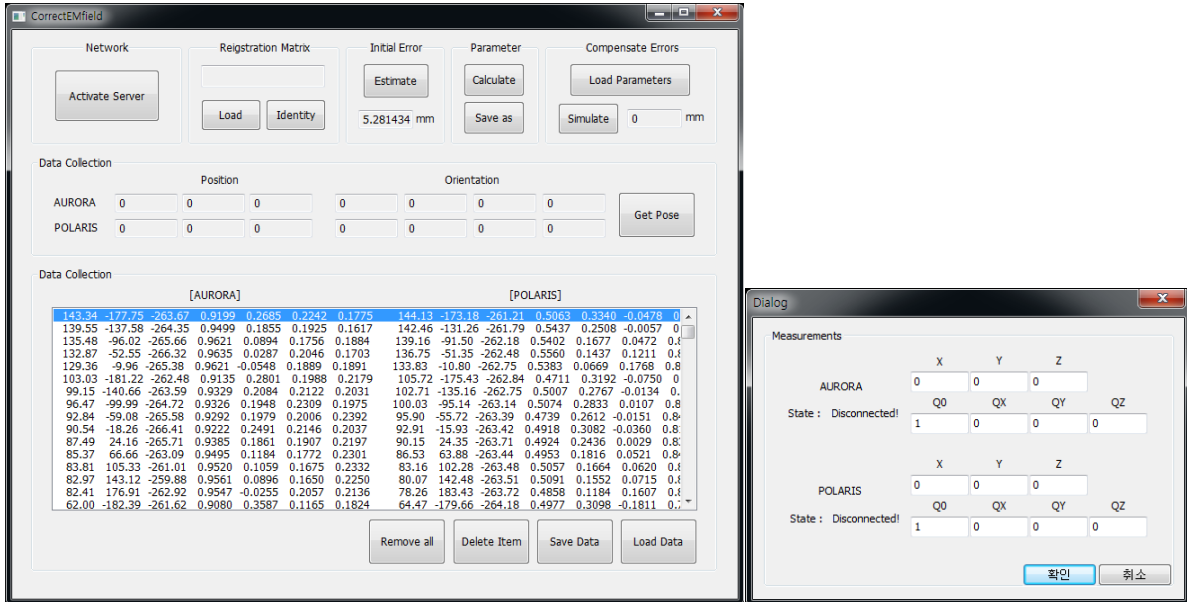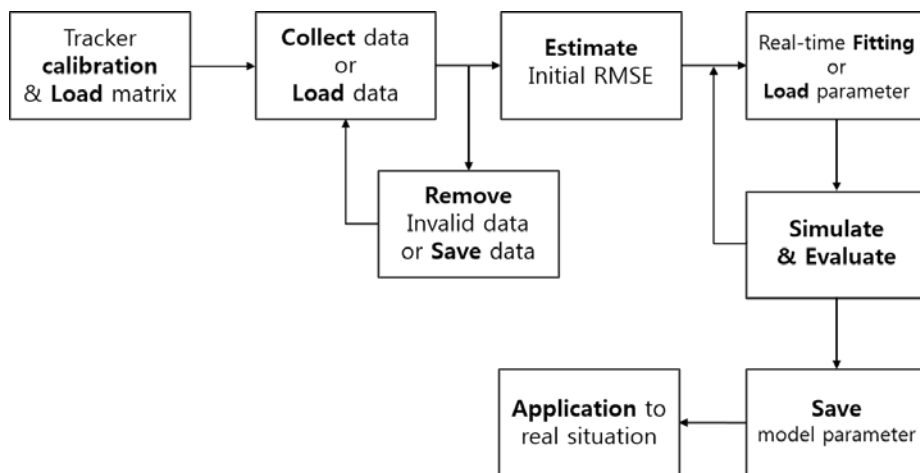
Ⅲ. Experiments

3.1 Experiment 1: Evaluation and Compensation of Error Field

Data Collection

To evaluate inherent tracking error of an EMTS which increases proportionally to the distance between the field generator and the coil sensor, Position data from an EMTS and an OTS was acquired by placing the probe tool at 60 points of known location on the calibration grid shown on Fig 3.1 and collecting the position values reported by each tracking system in a quasi-static manner. The OTS data was used as ground truth values with the tracker calibration result between the EMTS and the OTS. The calibration probe designed for use in tracker calibration step was identically used in this step. By using the calibration probe with the tracker calibration result representing the pose relationship between an EMTS and an OTS, data collection is able to be performed simultaneously for both an EMTS and an OTS in a short time. To efficiently analyze error tendency according to each axis of the coordinate frame of an EMTS with minimum number of measurements, 20 measurements are acquired while moving the probe in z direction with x and y coordinates set to zero among the 60 measurements, another set of 20 measurements in y direction with x and z coordinates set to zero, and the left 20 measurements in x direction with y and z coordinates set to zero, as shown on Fig 3.2. Sampling interval was 20 mm. The tracking range of an EMTS in each axis are fully covered with this sampling interval and the aforementioned number of measurements.

Figure 3.1 Experimental setup for collecting measurements from an EMTS and an OTS.
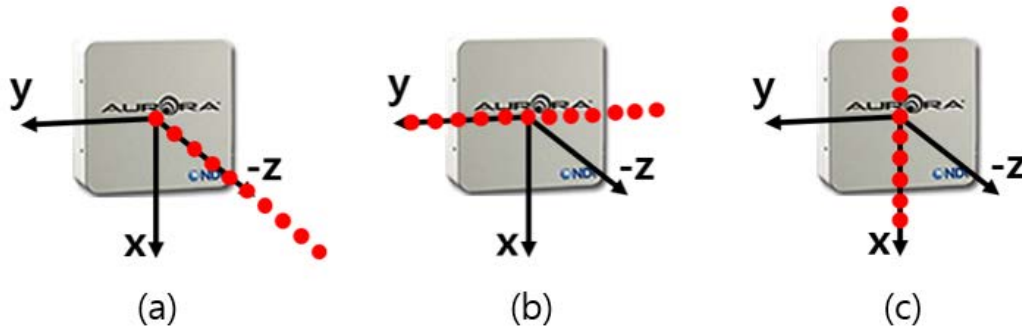
Figure 3.2 Data collection method for analysis on error according to each axis of the EMTS coordinate frame.

Error Evaluation and Correction

Based on each 20 measurement data, 1D deviations in each coordinate axis and 3D distance error without error correction are computed to provide min/max values and RMS values. We applied the simplified version of error correction algorithm described in the Methods chapter to compensate the error in an EMTS. To be specific, we set the basis function of the error polynomial as x^j instead of $x^{p'_j} y^{p''_j} z^{p'''_j}$ for the purpose of minimizing the number of measurements required to be taken for computing the unknown polynomial coefficients. The large number of terms, or coefficients in the polynomial could approximate the error field even closely, but collecting too many data in a long time is not suitable for use in clinical environments. We conducted polynomial fitting with the 2nd order to 6th order and compared the corrected data with the distorted EMTS data.

3.2 Experiment 2: Evaluation of Registration Accuracy

To evaluate the proposed system, we performed phantom experiments. A torso mannequin combined with L-spine phantom is prepared. The CT data of the phantom was prepared with 2.5-mm slice thickness, as shown on Fig 3.3. Fiducial markers attached to the surface of the torso mannequin were used as fiducial points in the patient-to-image registration. One of fiducial markers attached to the spine phantom was used as TRE measurement point. In the first experiment for evaluating the EMTS-based navigation system, the phantom [patient] were tracked in real time with the attached coil sensor by the EMTS, and the relative pose of the magnetic probe with respect to that of the phantom was defined as a patient fiducial point. Based on PPR method, registration was performed by using the patient fiducial points and the image fiducial points extracted in the CT image set of the phantom loaded in 3D Slicer. Fiducial registration error (FRE) was measured with 20 registration trials and target registration error (TRE) were estimated 20 times on the predefined point shown on Fig 3.4.

In the second experiment for evaluating hybrid navigation system, tracker calibration was performed prior to patient-to-image registration. Based on fiducial points located near the field generator (FG) reported in both coordinate frames of the EMTS and the OTS, calibration matrix was computed by PPR method. After that, patient-to-image registration was performed by using an OTS probe and an optical reference marker attached to the phantom. Finally, the tracking data of the magnetic probe was transformed into the coordinate frame of the reference marker with use of the calibration matrix and visualized in the image space by using the registration result. The rest of the experimental setup was the same as that of EMTS-based navigation system and the measurement of FRE and TRE was repeated 20 times.
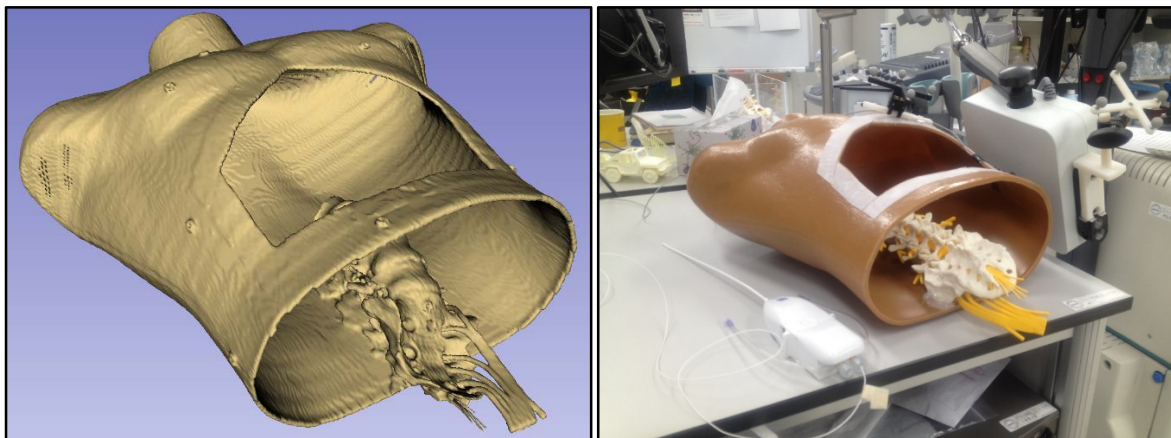
Figure 3.3 Torso mannequin combined with L-spine phantom prepared for the experiments.

In the last experiment, the accuracy improvement of hybrid navigation system by applying error correction technique was evaluated. In the same setup with hybrid navigation system, position data was randomly collected in a quasi-static manner near the TRE measurement site. With the collected data, error was modeled by using the 6th order polynomial fitting. The corrected position data was applied to the final transformation matrix transmitted to 3D Slicer and TRE was measured with the corrected transformation matrix representing the pose of the probe. 30 measurements are acquired for error modeling in each trial, and the trial number was 20.
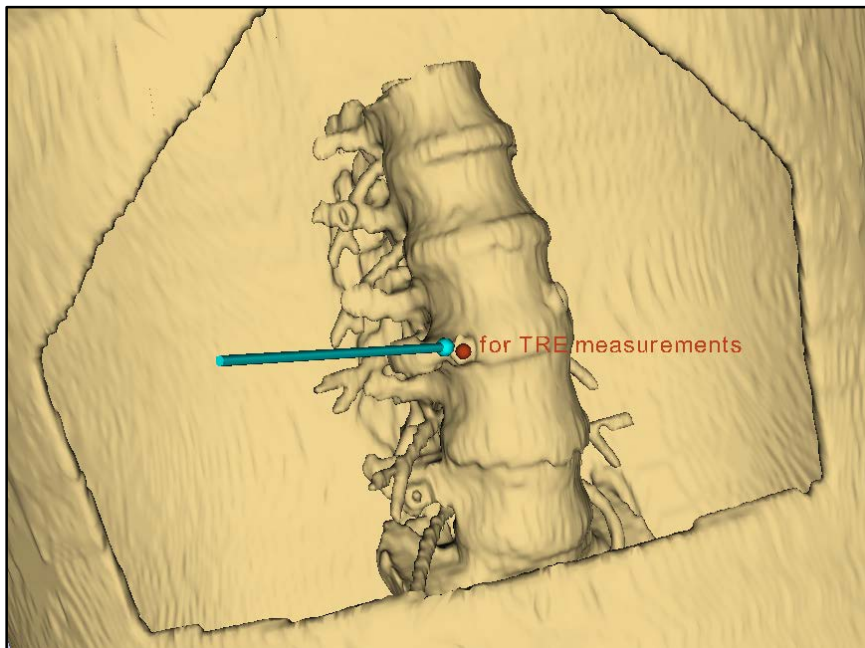
Figure 3.4 TRE measurement site identified on the 3D volume model reconstructed from the CT images.

Ⅳ. Experimental Results

4.1 Evaluation and Compensation of Error Field

We examined inherent tracking error in an EMTS by taking measurements in one axis direction with the other two coordinates set to zero. We conducted error fitting with the 2nd order to 6th order polynomials and compared the corrected data with the distorted EMTS data. Fig 4.1, 4.2, and 4.3 describes the increasing 3D distance error according to the separation in each direction between the field generator (FG) and the coil sensor. As shown on Table 4.1, 4.2, and 4.3, the maximum distance error in z variation was reduced from 10.333 mm to 4.555 mm by error correction and the RMS value also decreased from 6.821 mm to 2.399 mm. The maximum distance error in y variation was reduced from 16.802 mm to 2.287 mm by error correction and the RMS value also decreased from 6.995 mm to 1.061 mm. The maximum distance error in x variation was reduced from 4.160 mm to 1.299 mm by error correction and the RMS value also decreased from 8.167 mm to 2.295 mm. The degree of error reduction shows no significant difference in different polynomial orders, but the efficiency of error correction improved minutely according to the increasing polynomial order.
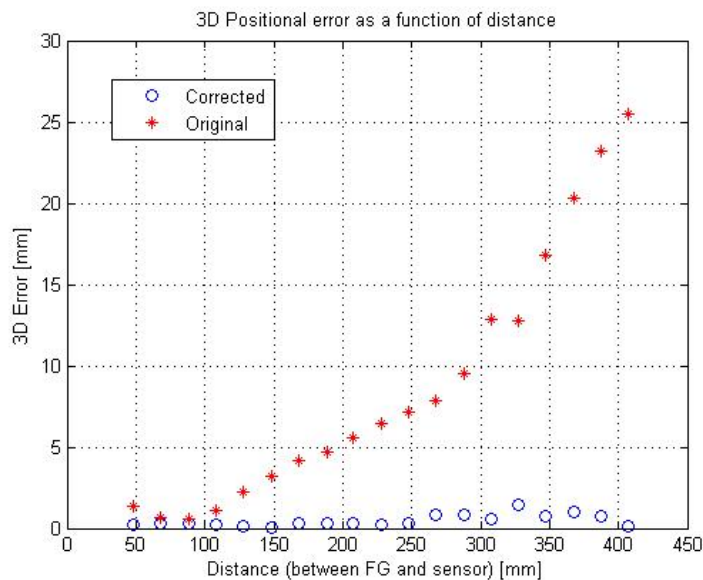

Figure 4.1 3D positional error affected by varied z coordinates with x and y coordinates set to zero.

Value [mm]		Raw	Fitted by the polynomial of the order				
			2	3	4	5	6
x	RMS	5.556	1.018	0.993	0.922	0.863	0.861
	min/max	1.780 / 6.310	0.017 / 1.858	0.011 / 1.907	0.007 / 1.659	0.053 / 1.520	0.089 / 1.521
y	RMS	2.459	1.573	1.486	1.485	1.480	1.468
	min/max	0.150 / 6.130	0.001 / 4.355	0.008 / 4.076	0.001 / 4.078	0.090 / 3.945	0.012 / 3.863
z	RMS	3.099	1.784	1.782	1.777	1.774	1.691
	min/max	0.020 / 5.420	0.035 / 4.378	0.036 / 4.430	0.111 / 4.570	0.031 / 4.475	0.004 / 4.552
d	RMS	6.821	2.587	2.523	2.493	2.466	2.399
	min/max	2.768 / 10.333	0.460 / 4.724	0.318 / 4.544	0.289 / 4.596	0.299 / 4.481	0.360 / 4.555

Table 4.1 Comparison of the corrected data fitted by the polynomial of the 2nd to 6th order with the distorted data with z coordinate variation.

Figure 4.2 3D positional error affected by varied y coordinates with x and z coordinates set to zero.

Value [mm]		Raw	Fitted by the polynomial of the order				
			2	3	4	5	6
x	RMS	2.835	1.739	0.698	0.693	0.691	0.684
	min/max	0.030 / 9.280	0.016 / 4.074	0.004 / 1.399	0.005 / 1.392	0.004 / 1.421	0.022 / 1.491
y	RMS	1.142	0.911	0.895	0.895	0.813	0.737
	min/max	0.060 / 2.780	0.033 / 1.883	0.021 / 2.027	0.035 / 2.027	0.058 / 1.729	0.026 / 2.228
z	RMS	6.292	0.485	0.463	0.460	0.456	0.341
	min/max	0.010 / 15.940	0.045 / 1.105	0.018 / 1.105	0.017 / 1.087	0.045 / 1.079	0.001 / 0.725
d	RMS	6.995	2.023	1.226	1.222	1.160	1.061
	min /max	0.435 / 16.802	0.256 / 4.470	0.207 / 2.040	0.271 / 2.030	0.347 / 1.730	0.310 / 2.287

Table 4.2 Comparison of the corrected data fitted by the polynomial of the 2nd to 6th order with the distorted data with y coordinate variation.
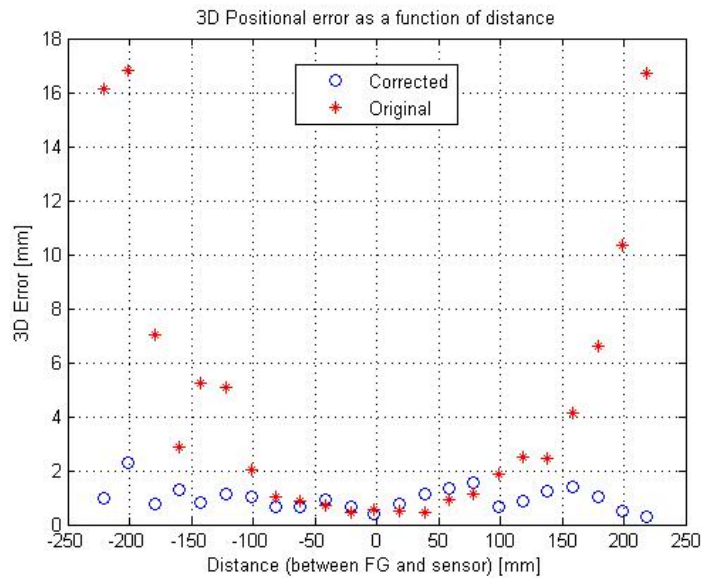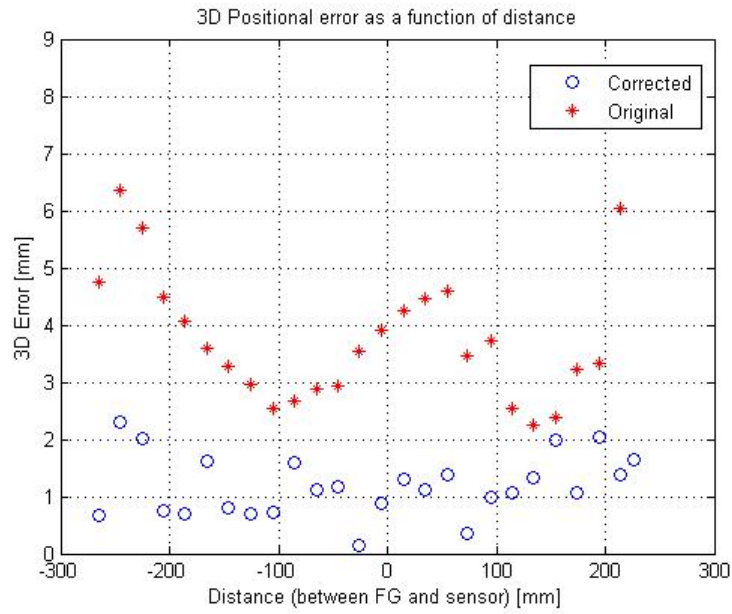
Figure 4.3 3D positional error affected by varied *x* coordinates with *y* and *z* coordinates set to zero.

Value [mm]		Raw	Fitted by the polynomial of the order				
			2	3	4	5	6
x	RMS	2.111	1.311	0.947	0.842	0.842	0.615
	min/max	0.040 / 6.440	0.025 / 2.595	0.120 / 2.012	0.001 / 1.874	0.007 / 1.886	0.053 / 1.183
y	RMS	3.388	1.037	1.024	0.983	0.952	0.946
	min/max	1.430 / 5.600	0.041 / 2.381	0.050 / 2.422	0.006 / 2.109	0.001 / 2.109	0.001 / 1.999
z	RMS	1.169	0.829	0.829	0.825	0.733	0.645
	min/max	0.020 / 3.380	0.018 / 2.152	0.011 / 2.144	0.013 / 2.208	0.041 / 1.752	0.003 / 1.611
d	RMS	4.160	1.866	1.866	1.535	1.467	1.299
	min/max	2.245 / 8.167	0.588 / 3.144	0.436 / 3.156	0.363 / 2.822	0.320 / 2.955	0.152 / 2.295

Table 4.3 Comparison of the corrected data fitted by the polynomial of the 2nd to 6th order with the distorted data

with *x* coordinate variation.

4.2 Evaluation of Registration Accuracy

We compared accuracies of EMTS-based navigation system and hybrid navigation system in terms of FRE with 20 trials, and accuracies of EMTS-based navigation system, hybrid navigation system in terms of TRE with 20 trials. Figure 4.4 shows the registration accuracies of each system. The average FRE of EMTS-based navigation system was 2.60 ± 0.37 mm and that of hybrid navigation system was 1.46 ± 0.27 mm. The average TRE of EMTS-based navigation system was 3.15 ± 0.50 mm, that of hybrid navigation system was 2.17 ± 0.34 mm, and that of hybrid navigation system with error correction was 1.48 ± 0.51 mm. The average registration error in EMTS-based navigation system was meaningfully decreased by 1.14 mm for FRE and 0.98 mm for TRE. Error correction with the polynomial fit method further reduced the average TRE of hybrid setup by 0.69 mm.
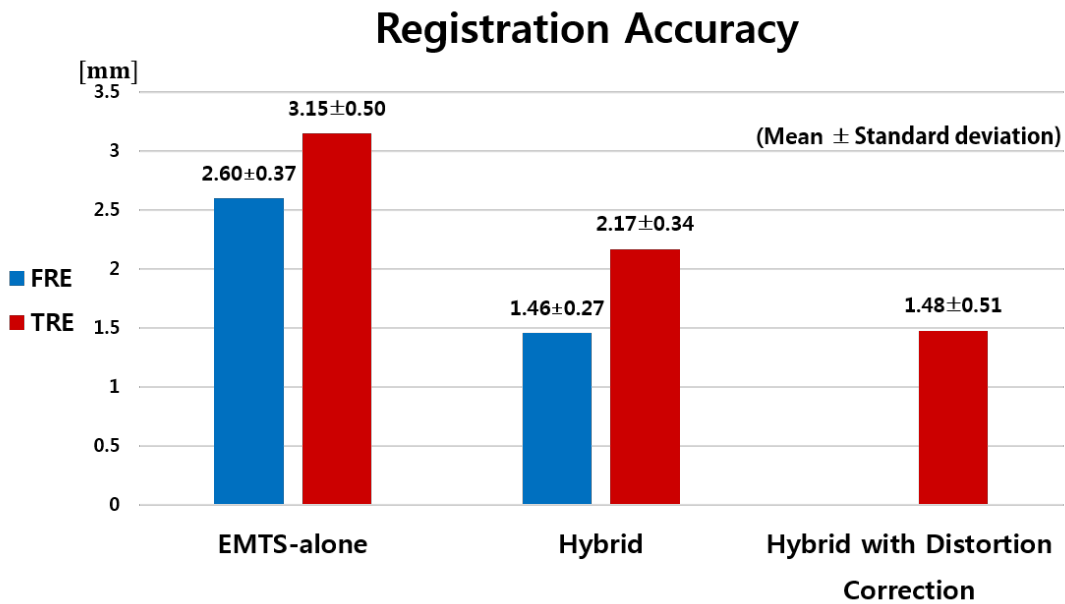

Figure 4.4 Registration accuracies of EMTS-based, hybrid, and hybrid with error correction.

Ⅴ. Clinical Application

5.1 Epiduroscopic Laser Neural Decompression (ELND)

As presented in the foregoing, ELND is a surgical procedure which ablates the target lesion by applying laser under guidance of endoscopic view. For performing ELND, a flexible and steerable video-guided catheter is commonly used which provides two working channels within it. A laser fiber and a fiber endoscope can be accommodated in each working channel, which means that the operating surgeon can perform catheter ablation while directly viewing the target lesion or the internal anatomy of the surgical patient in real time. In this regard, ELND is highly effective for treatment of LBP or lumbar herniated intervertebral disc disease. However, limited field of view and relatively low resolution of the images from the flexible endoscope raise the need to use fluoroscopy, which is a kind of X-ray imaging, for the purpose of localizing the position of the catheter tip inside the patient body. Continuous or discrete fluoroscopic images are provided during the whole procedure at a heavy cost of radiation exposure for both surgeons and the patient. The following describes the overall flow of the conventional ELND procedure.

1. Position the surgical patient in prone position on the surgical bed.
2. Sterile the lumbosacral region of the patient.
3. Meanwhile, set up epiduroscope or fiber endoscope and adjust the focus of it.
4. Put the patient under general anesthesia.
5. Puncture the sacral hiatus with Tuohy needle in 45 degree angled and advance Tuohy needle in 20-30 degree angle.
6. Insert guide wire through Tuohy needle and remove the needle.
7. Confirm the pathway by identifying the guide wire in a G-arm fluoroscopic image.
8. Make a 1 cm longitudinal skin incision.
9. Widen entry portal with smooth awl.
10. Remove the guide wire and insert steerable catheter with the fiber endoscope and the laser-emitting fiber in each working channel of the catheter.

11. Advance the catheter under guidance of fluoroscopy and endoscopy to reach the target lesion.

12. Conduct laser ablation of the target lesion with the direct view of it from the endoscope while doing saline irrigation to lower the heat from laser. In case of END, perform direct steroid injection through the working channel.

13. Suture the skin incision.

5.2 Navigation-Guided ELND

We have tried clinical use of our navigation system in the real operating room over 10 patients. Our navigation system aims at (1) providing surgeons with 3D visual information on positional relationship between the patient anatomy and the surgical tool (video-guided catheter) to enable the procedure to be performed fast, safely, and successfully and (2) replacing fluoroscopy totally or in part to reduce the amount of X-ray radiation to which both surgeons and the patient have to be exposed during the procedure. From here, we are going to describe the requisite steps and some crucial considerations on each step for performing surgical navigation in ELND.

5.2.1 Preoperative Preparations

Preparation of Sensors

At the very first time, we should prepare corresponding number of sensor sets according to the number of surgical patients since a sterilized sensor set has to be used only once for one surgical patient. If sterilization of surgical tools can be done on the spot, we can use one sensor set repeatedly for multiple surgical patients. However, it is not allowed in the real situation since sterilization process takes certain period of time more than several hours. Once, abrupt breakdown of one of the prepared sensor set took place in the middle of procedure and thus we could not resume surgical navigation any more due to lack of a spare sensor set which had been sterilized ahead of time. In this regard, extra sensor sets should be prepared in the operating room so that they can be alternatively used in case of abrupt malfunction of the pre-allocated sensors during the procedure. For intraoperative use of sensors, we should prepare tool definition files of the sensors in advance. The tool definition file contains geometry information of a sensor required for the tracker grasping the pose of the sensor. Aurora sensors used as a reference don't need any tool definition files since tool information is pre-programmed

in the SROM device. In case of probe tools of both Aurora and Polaris, there generally exists some locational difference between the tip of the probe and the attached sensor. Such offset is calculated via pivot calibration process and that information is stored in the tool definition file as well as information on the sensor geometry itself. Once a tool definition file for a sensor is generated prior to the procedure, the shape of the sensor must be consistent during the whole procedure since a tracking system is able to normally track the pose of the sensor only based on information from the tool definition file of the sensor. This is the reason why geometrical deformation of a sensor due to sterilization with high pressure and temperature inhibits the sensor from being normally tracked by the tracking system during the procedure.

Sterilization of Sensors

All materials which are supposed to be used and in direct contact with the patient body during the procedure must be handed over to the relevant staff belonging to the operating room one day before the surgery and sterilized in order to guarantee aseptic condition of sensors via sufficient duration of sterilization. It is also important to check whether relevant tools or sensors are manufactured so that they can withstand high temperature and pressure without any geometrical deformation or breakdown during the autoclave sterilization. In our case, we designed and manufactured sensor frames to fit into our own application by using rapid prototyping (RP) machine. However, we found that they were considerably deformed after sterilization, so their pose could either be tracked with a great amount of tracking error or not be tracked by the tracking system any more. In this respect, selection of material for manufacturing sensor frames or tools is an important issue. In case of complete products from NDI corporation including electromagnetic coil sensors of AURORA system and retro-reflective optical markers of POLARIS system, the manufacturer specification suggests 20 cycles as a limited number of sterilization for AURORA sensors and nothing for POLARIS optical markers. In our clinical trials, we confirmed that they works normally after sterilization via autoclave within the announced limitation number.

Preoperative CT Scanning

As a prerequisite for performing surgical navigation, coordinate systems of the real world [patient] and the medical image [CT] should be registered each other to display . This process are usually called patient-to-image

registration. There are several kinds of registration methods including point-based registration, surface matching, image-based registration, and so on. Among them, we adopted the point-based one as the registration method in our navigation system in that it provides both reliable accuracy and ease of operation in a balanced way.

For identifying and matching corresponding feature points in both the real world and the image, anatomical landmarks or artificial skin markers are used as fiducial points used for registration. In our case, we manufactured round-shaped fiducial markers by using RP machine as shown on Fig 5.1. The marker was designed to be tiny (Outer diameter: 15mm) and to have a small hole in the middle of the marker to facilitate taking measurements of the marker location by using the probe in the registration step. A group of these markers are attached to the patient skin in a manner of encircling the surgical site in order that the center of gravity of markers' dispersion is located near the surgical site for getting better TRE. If markers are distributed on the skin surface of the patient with their geometry of a flat plane, the registration accuracy in the deeply seated area inside the patient could get lower despite acceptable range of registration accuracy in the skin surface. After proper arrangement of fiducial markers, the surgical patient receives CT scanning with the markers attached to his or her skin, and then the markers can be identified in the CT images to be used as fiducial points in the image space.

Figure 5.1 Arrangement of fiducial markers identified in the CT image set.

The time interval between CT scanning and surgery should be minimized as short as possible in that the difference of anatomical geometry of the patient in CT scanning and surgery could negatively affect the navigation accuracy. However, it is not allowed at times due to various conditions of a hospital. In that case, some of the skin markers could slightly move from their original location during the waiting time, which generates

FLE, consequently degrading the resultant registration accuracy. In addition, in case of some markers being detached during the waiting time, insufficient number of available fiducial markers could limit the registration process. In this regard, as depicted on the figure, it is necessary to mark the position of skin markers with a color pen in case that the attached markers become detached before the surgery begins.

The pose of the patient when receiving CT scanning is also an important factor to possibly affect the registration accuracy. In general, patients are required to be in the supine position in CT or MR imaging. However, if the same manner is applied to the ELND patient, there could be a noticeable difference between the spine geometry of the patient in the surgical procedure and preoperative CT scanning since the patient goes through ELND procedure in the prone position, which could result in significant navigation error or TRE. Thus, the surgical patient in preoperative CT scanning should be controlled to be in the same prone position as the pose of the surgical patient in the surgical procedure to minimize the aforementioned error.
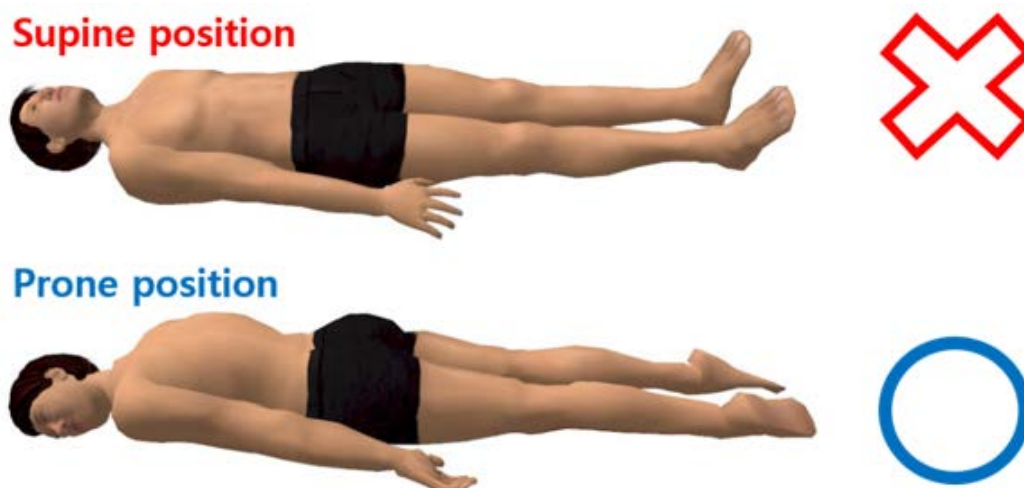

Figure 5.2 Pose of an ELND patient in preoperative CT scanning.

Moreover, field of imaging should be adequately adjusted when the radiologist generates image data to guarantee that all the skin markers are identified in the CT image set. Depending on the surgical situation, some marker omissions in the image could impede patient-to-image registration process by causing the number of fiducial points required for the acceptable range of registration accuracy to be insufficient. Another possible problem related to the field of imaging is intentional degradation of the image resolution in the axial direction, which leads to a big slice thickness, for the purpose of avoiding the excessive amount of CT slices to be processed. This case could take place when imaging field is adjusted so as to cover unnecessarily broad area in the

patient body. In fact, the whole vertebral column doesn't need to be covered in CT scanning since the surgical site of interest in ELND is typically confined to a limited area including only two to three lumbar vertebrae adjacent to each other. In this regard, proper adjustment of imaging field is highly required to obtain acceptable image resolution together with moderate number of CT slices. According to our experiences, we recommend that slice thickness of the image set should be no more than 2.0 mm assuming that the imaging field of scanning is properly set up. The slice thickness ranging from 1.0 mm to 1.5 mm would be a suitable value in that, in case of a small value of slice thickness, there is no need to perform post-processing of the image such as resampling the image data based on various interpolation techniques required for enhancing the image resolution in the axial direction and generating smoother 3D model of the patient anatomy, by which errors resulting from mod-ification of the original image could be generated additionally.

The file format of the image acquired from CT scanning must be DICOM, which is short for Digital Imaging and Communications in Medicine and is a standard for handling, storing, printing, and transmitting information in medical imaging. Only the image set in DICOM format can be loaded and used for performing surgical navigation in our visualization platform that is 3D Slicer.

Preoperative Surgical Planning

The surgical planning is the preoperative process which visualizes a surgical intervention in order to prede-fine the surgical steps prior to the surgical procedure. Surgical planning includes the followings: Reconstructing a 3D model from a medical image set, segmenting certain anatomical structures of interest in the surgery from the whole 3D image set, and planning the optimal path where the surgical tool should proceed by referring to the anatomical structure from the medical images. The preoperative surgical planning can be transferred to the real operating theatre via surgical navigation system, yielding more successful outcome of the surgery. In this regard, preoperative surgical planning is one of the most important steps in performing surgical navigation.

In our trials, extraction of the whole vertebral column by applying the intensity-based segmentation method based on adjustment of the intensity threshold is performed at the first stage of the planning. Depending on situations, image interpolation is performed in case that a big slice thickness hinders the vertebral column from being extracted clearly from the CT image set to reconstruct a smooth 3D model. Moreover, if adjacent tissues in nearby places have the similar range of image intensity to that of the spine, a series of erosion and dilation filtering should be followed together with some manual editing work, or erasing to get rid of the adjacent tissues

acting a noise. At this moment, the ilia are apt to be extracted together with the vertebral column due to the intensity similarity. In this case, it is highly recommended to eliminate the unnecessary anatomy, or the ilia from the initially segmented 3D model since the ilia hides the pathway of the catheter on the navigation display, as shown on the Fig 5.3. Additional segmentation, or labeling with some unique colors of the target lesion, the intervertebral disc adjacent to the surgical target, nearby nerves or blood vessels could be also helpful for surgeons to advance the catheter to reach the target safely and efficiently.

Finally, prior acquisition of coordinate data of fiducial points in the CT image space are performed to enable the registration procedure to be conducted rapidly during the procedure. For preventing any mistakes or time delay from occurring in the procedure, it is recommended to prepare the data with certain order which guarantees that surgeons can easily obtain the patient's position data using the probe tool in the registration step without being confused.

Skin marker segmentation is also recommended for the following two reasons. First, surgeons are able to identify the catheter tip position much better with marker positions as a visual reference. Second, surgeons can estimate the registration accuracy with ease right after patient-to-image registration by locating the tip of a probe or a catheter on the center hole of the marker and examining the positional disparity between the tool and the marker shown on the virtual 3D space, or the navigation display. After that, adequate actions could be followed such as re-performing the patient-to-image registration or, if the error shows the unidirectional tendency of bias, applying some offset value in the corresponding direction to the pose data of the catheter in real time.
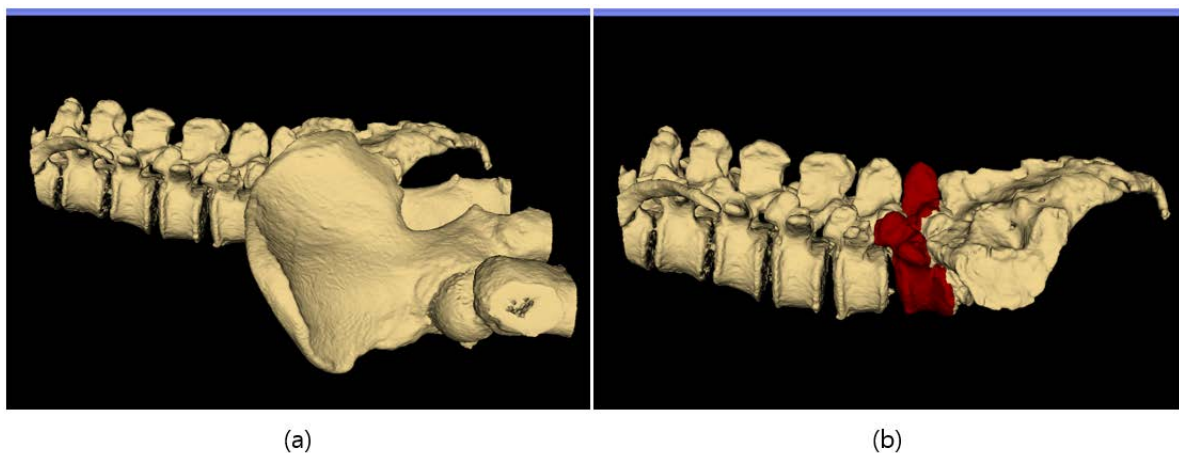

(a)   (b)

Figure 5.3 3D model of the vertebral column (a) before and (b) after eliminating the ilia with target labeling.

5.2.2 Intraoperative Set-up for ELND Navigation

Once all the aforementioned arrangements are done before the surgery, intraoperative set-up of the navigation system begins from the time clinical staffs and a surgical patient enter the operating room.

First, the surgical patient is put under general anesthesia, while being in the prone position on the surgical bed. In general, it takes several minutes, sometimes more than ten minutes for the patient to be under complete anesthesia. Meanwhile, engineers arrange the navigation system including optical tracking system, electromagnetic tracking system, and navigation workstation in the operating room. Environment of the operating room is usually complicated due to considerable number of clinical staffs as well as medical devices including G-arm unit, laser system, endoscope system, and the like. Accordingly, tracking systems should be properly located so that their tracking functionality is not impeded by presence of the aforementioned components of the operating room. The figure depicts is our configuration of the system arrangement in the operating room.

In the meantime, staffs sterilize the skin of lumbosacral region of the surgical patient. In the conventional ELND procedure, The back of the patient is often covered with sterile surgical drapes except for the small region surrounding the entry portal of the catheter. In case of performing surgical navigation, some space for the attached skin markers as well as the entry portal should be maintained without being covered with the drape since the markers are supposed to be accessed by the probe in the registration process. For the minimum level of hygiene, the exposed marker area is sometimes covered by a self-adhesive vinyl drape which is very thin and transparent so that color markings of the skin markers are visible through the drape. Thereafter, attachment of sensors on the patient skin is allowed to be done after the aforementioned sterilization process because all sensors have been maintained in the aseptic state since the prior autoclave sterilization. At this point, one crucial task is to check whether the attached sensors are being tracked normally in the tracking volume or not. Furthermore, it is also recommended to check if the sensor is located close to the field generator enough that the current location of the magnetic coil sensor yields sufficient tracking accuracy, considering that accuracy of measurements from the magnetic coil sensor gets lower as the distance between the field generator and the coil sensor increases. If not, either the sensor on the patient skin or the field generator should be rearranged. After rearrangement of the field generator, it should be covered with sterile surgical drape to avoid direct contact with the patient body, as shown on Fig 5.4.
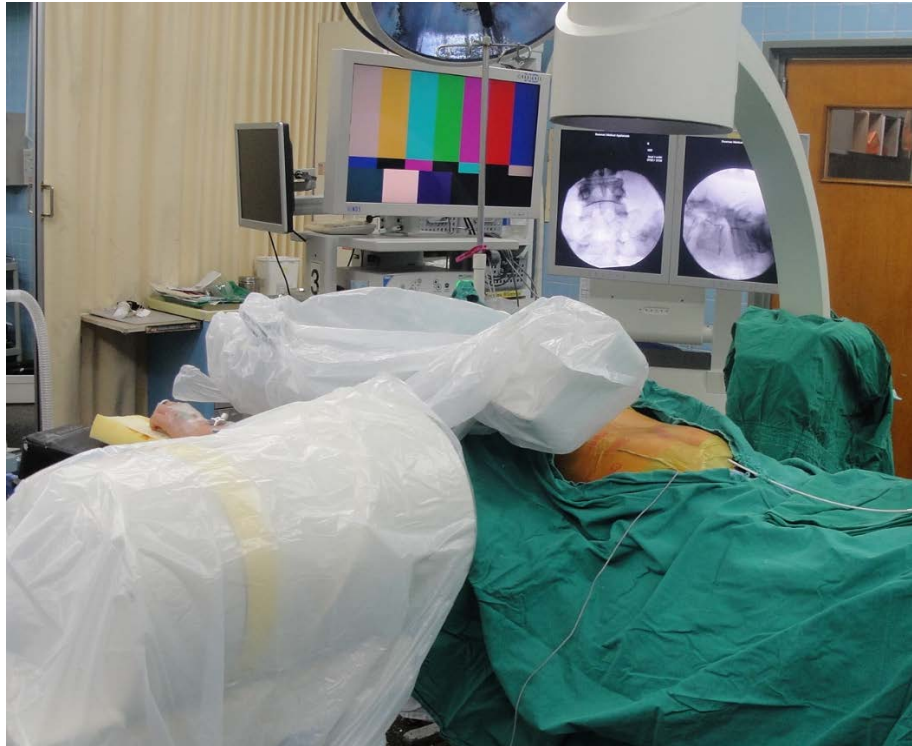
Figure 5.4 Field generator covered with sterile surgical drape. Cable sensor is located close to the field generator enough to generate acceptable tracking accuracy.

Meanwhile, epiduroscope, or flexible endoscope is set up and its focus is adequately adjusted by surgeons. Once the aforementioned things are done, all we need for tracker calibration and patient-to-image registration process are prepared.

The tracker calibration is a process for calculating the positional relationship between the EMTS and the OTS. To be specific, an optical marker is attached to the field generator of the EMTS and a homogeneous transformation matrix representing the relationship between the optical marker and the field generator is calculated based on paired point registration method. Once we know the relationship via tracker calibration, the pose of the catheter-type magnetic sensor can be reported in the OTS coordinate frame in real time and the patient-to-image registration matrix which is obtained with high accuracy by using the OTS can be used in our navigation system, thus yielding better navigation accuracy. For the purpose of avoiding time delay and facilitating the calibration process during the real procedure, we designed a calibration probe which enables measurements to be taken at the same time in both coordinate systems of the EMTS and the OTS. As shown on Fig 5.5, an optical marker set and a magnetic coil sensor are integrated in a single body and the tracked positions of the optical marker and the coil sensor aligned to be the tool tip of the probe via pivot calibration.

After tracker calibration, patient-to-image registration is followed right after conducting tracker calibration, as shown on Fig 5.6.
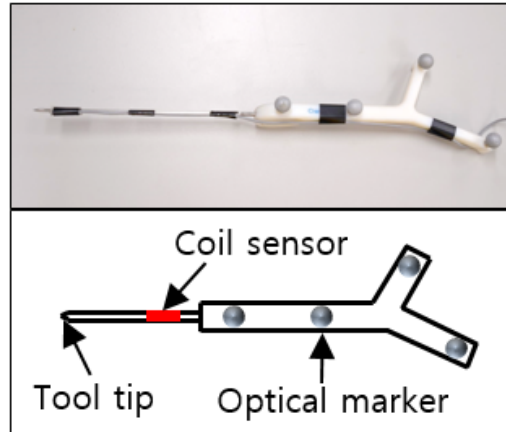

Figure 5.5 Calibration probe designed to intra-operatively perform tracker calibration fast and conveniently.
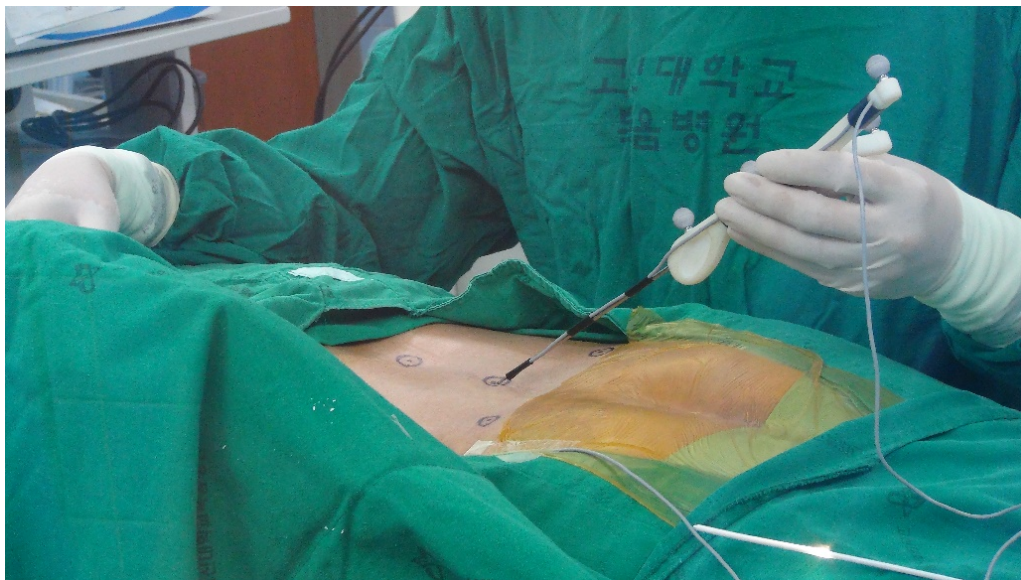

Figure 5.6 Acquisition of patient fiducial points used for patient-to-image registration.

According to our experiences, time-consuming registration procedure had to be re-performed many times in case that the reference sensor attached to the patient skin are detached or abruptly breaks down to make the pre-calculated registration matrix being useless. For avoiding such a time delay during the procedure and re-suming surgical navigation in spite of sudden breakdown of the reference sensor, we need to perform patient-to-image registration considering performance of surgical navigation both with and without the reference sensor.

Two cases of registration matrices are simultaneously acquired by using simple matrix algebra in the navigation software as follows. In addition, a functionality of performing registration using the catheter-type sensor is also included in the navigation software in case that the probe tool cannot be used any more due to various reasons such as breaking down or being dropped to be in the septic state. All of the intraoperative steps above mentioned must be performed with only surgeons, since engineers cannot have access to all of sterilized materials including the sensors.

After patient-to-image registration process, estimation of the registration result is done, as shown on Fig 5.7, by locating the tip of a probe or a catheter on the center hole of the fiducial marker and examining the positional disparity between the tool and the marker shown on the virtual 3D space, or the navigation display.

Figure 5.7 Navigation accuracy assessment with the probe or the catheter placed on the fiducial points on the patient skin after finishing the registration step.

After that, adequate actions could be followed such as re-performing the patient-to-image registration or, if the error shows the unidirectional tendency of bias, applying some offset value in the corresponding direction to the pose data of the catheter in real time.

After the estimation is done and the relevant measures are taken, assistant surgeons make puncture of sacral hiatus with Tuohy needle (45 degree angled) or make a longitudinal skin incision (about 1 cm) around the sacral area and finally widen entry portal with smooth awl to facilitate insertion of the video-guided catheter.

5.2.3 Catheter Insertion under Guidance of Navigation

The operating surgeon enters the operating room. Video-guided catheter which has two channels within it is inserted through the incision. First, the video-guided catheter is equipped with the fiber endoscope and the catheter-type magnetic sensor in each working channel. The catheter is advanced under guidance of virtual reality-based navigation instead of fluoroscopy in the conventional procedure until it reaches the target lesion area. The navigation system provides a 3D view showing the positional relationship between the patient anatomy, or the spine and the surgical tool, or the catheter in the virtual space. However, many of surgeons are basically accustomed to image analysis based on 2D imaging modality such as X-ray imaging or fluoroscopic imaging. In that regard, we decided to provide a functionality of 2D slice-based navigation together with 3D model-based navigation in our navigation system. As depicted on Fig 5.8, the location of the tool tip is displayed in the shape of cross hairs on multi-planar reconstruction (MPR) images based on each anatomical plane as well as in the 3D virtual space.
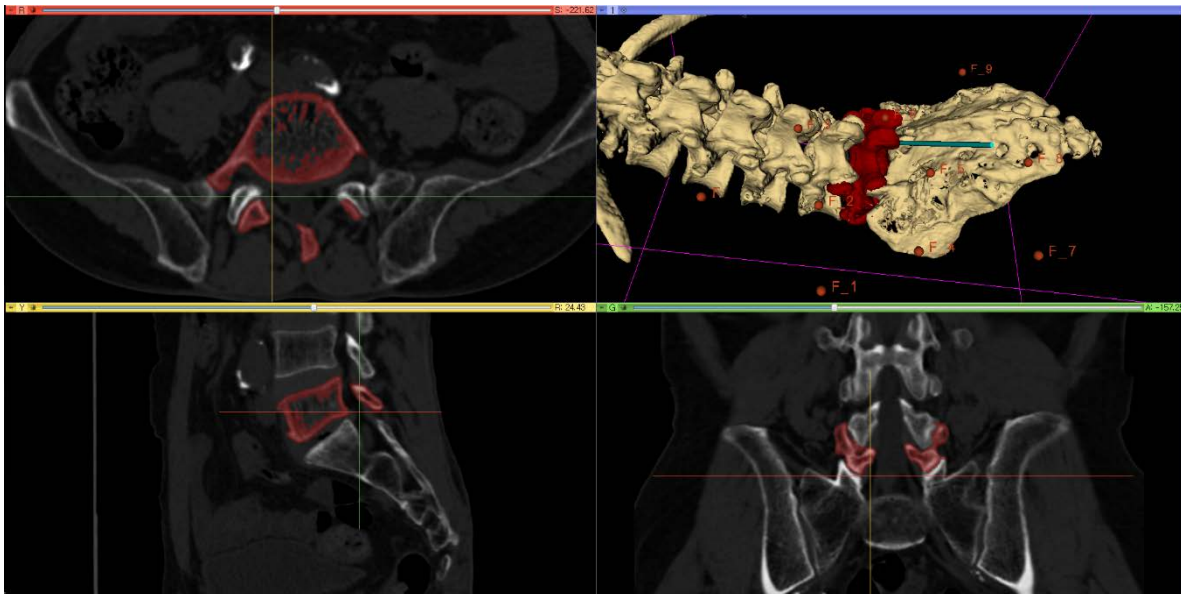

Figure 5.8 Navigation display providing both a 3D view and MPR image-based 2D view.

Even though the CT images of the patient are initially acquired in the axial plane of the patient, MPR allows images to be created from the original axial plane in either the coronal or sagittal plane. 3D Slicer that we adopted as our basic visualization platform in the navigation system basically provides a functionality of MPR. Real-time switching of various display layout including 3D only, 3D with three MPR images, or single MPR

image only is also available in 3D Slicer. When the surgeon judges on information from the navigation system that the catheter nearly gets to the surgical target, a couple of fluoroscopic imaging could be performed to finally confirm that the tip of the catheter is actually located in the target site, as shown on Fig 5.9.
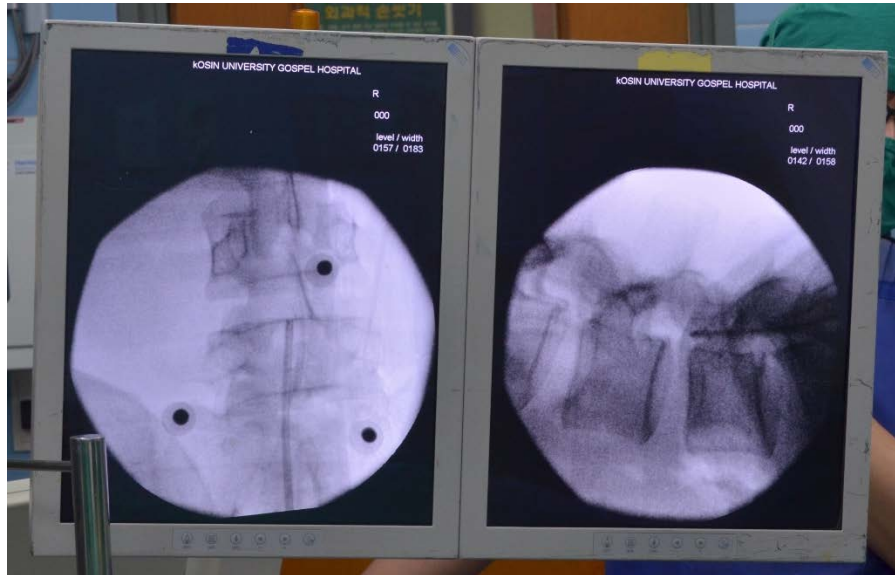

Figure 5.9 Video-guided catheter identified on the bi-planar fluoroscopic images.

After final placement of the catheter is done accurately, the magnetic sensor is removed from the working channel and the laser-emitting fiber is inserted in that channel and then the operating surgeon performs laser ablation of the target lesion, while viewing the real-time endoscopic images. In general, laser ablation takes a short time around five to ten minutes to be completed. Finally, the video-guided catheter is removed and the skin incision is closed.

5.2.4 Discussion on Clinical Application

The far distance between the field generator and the coil sensor was one of the most influential error-causing factor. Complicated surgical environments often impede adequate positioning of the field generator. Inadequate arrangement of skin fiducial markers on the patient skin also causes registration error to be large. It is recommended that center of mass of a fiducial marker set be close to the surgical target as much as possible to acquire the best registration accuracy. Sensor frames manufactured by rapid prototyping (RP) were deformed after sterilization due to its high temperature and pressure. Such deformation causes tool tracking based on the predefined

tool geometry to be inaccurate. Thus, rigid materials that are not deformed by sterilization should be selected for manufacturing sensor-related tools. Disagreement between patient's poses in CT scanning and in surgical procedures gives rise to some degree of registration error. In general, patients are in supine position when receiving CT scans. However, patients of ELND should receive CT scans in prone position since the surgical patient of ELND procedure is positioned in prone position. If not, geometry of the spine has some difference in two cases, causing navigation error. In addition, fiducial points (used for registration) with a high error indication value could negatively affect the registration accuracy. The indication value is provided by the tracking system and selective acquisition of points with low indication value could reduce possible registration errors. In a practical aspect, detachment or displacement of the patient reference sensor after registration is a crucial problem. Since registration is usually conducted based on the coordinate frame of the reference sensor, small range of displacement could cause some navigation error, and in case of large displacement or detachment, registration must be re-conducted, which is a time-consuming task and is generally not allowed in pressing clinical situations. For this reason, registration result which does not allow for existence of the reference sensor should be acquired together with that allowing for the reference sensor. The operating surgeon gives us some positive remarks on qualitative estimation of our navigation system, but we did not acquire quantitative data on accuracy of the system yet due to the limited operating time.

Ⅵ. Discussions

The proposed navigation system is expected to replace fluoroscopy used in ELND procedures, highly reducing radiation doses for both surgeons and the surgical patient. Compared with EMTS-based navigation system, hybrid navigation system shows improved registration accuracy by making use of an accurate registration result which is obtained with use of an OTS. However, inherent tracking error of an EMTS still degrades the accurate registration result obtained by using an OTS in some degree. For that problem, error compensation by polynomial fit method alleviates such degradation, thus providing further improvement of navigation accuracy to hybrid navigation system. The designed calibration probe is an integrated type probe enabling simultaneous acquisition of tracking data from an EMTS and an OTS. With this probe, both tracker calibration and error correction can be conducted in a short time without a specially-designed calibration object. The result of tracker calibration is independent of locational change of the tracking systems since the EMTS is tracked in real time by the OTS, which is an encouraging aspect considering complicated real surgical environments. The transformation between coordinate frames of an EMTS and an OTS obtained by tracker calibration process needs to be optimized in terms of accuracy in that it highly affects not only navigation accuracy of hybrid navigation system, but also the effectiveness of the error compensation result. Error compensation was performed under the static condition that any magnetic interferences near the place of the experiment remain unchanged during the duration of the whole experiment. Error compensation was applied only to position error since orientation of the tool tip is unimportant information to surgeons in epiduroscopic procedures. In fact, they always focus on where the location of the catheter tip inside the patient body is. Error correction technique based on polynomial fitting does not require too many measurements to be taken, and thus takes a short time for data collection, while showing reliable performance, which is an encouraging aspect in terms of clinical application.

Ⅶ. Conclusions

In this study, a surgical navigation system for epiduroscopy was proposed, which aims at replacing fluoroscopy to reduce radiation doses for both surgeons and the surgical patient, and providing surgeons with accurate navigation information. For that purpose, a surgical navigation system was developed according to the following system development flow: (1) EMTS-based surgical navigation system in the initial stage, (2) hybrid navigation system in the intermediate stage, and (3) Hybrid navigation system with error correction in the final stage. We first performed the experiment for evaluating the inherent tracking error of an ETMS and the effectiveness of the error correction technique. After that, we performed the phantom experiments to compare accuracies of the systems in each development stage in terms of fiducial registration error (FRE) and target registration error (TRE). It is confirmed in the experiments that: (1) compared with EMTS-alone navigation system, hybrid navigation system provides improved registration accuracies by using an EMTS and an OTS in a complementary way, and (2) error correction based on polynomial fitting could further improve navigation accuracy of hybrid navigation system. Finally, clinical applications of the proposed system in ELND procedures were tried upon 14 ELND patients to assess feasibility of the proposed system.

References

[1]   M. S. BURMAN, "Myeloscopy or the direct visualization of the spinal canal and its contents," *The Journal of Bone & Joint Surgery,* vol. 13, pp. 695-696, 1931.

[2]   *www.myelotec.com*

[3]   J. D. Kim, J. H. Jang, J. Y. Kim, G. H. Jung, and S. J. Jang, "Epiduroscopic laser disc and neural decompression," *Journal of Neurosurgical Review,* vol. 1, pp. 14-19, 2011.

[4]   Y. K. Choi, M. H. Tan, J. D. Barbella, and W. R. Grubb, "Epiduroscopic analysis of persistent back and leg pain and the efficacy of epiduroscopy in the treatment of failed back pain syndrome," *REGIONAL ANESTHESIA AND PAIN MEDICINE,* vol. 26, pp. 90-90, 2001.

[5]   G. Schütze, *Epiduroscopy: Spinal Endoscopy*: Springer, 2008, pp. 70-77.

[6]   J. Boncher and W. F. Bergfeld, "Fluoroscopy‐ induced chronic radiation dermatitis: a report of two additional cases and a brief review of the literature," *Journal of cutaneous pathology,* vol. 39, pp. 63-67, 2012.

[7]   K. Komiya, T. Igarashi, H. Suzuki, Y. Hirabayashi, J. Waechter, and N. Seo, "In vitro study of patient's and physician's radiation exposure in the performance of epiduroscopy," *Regional Anesthesia and Pain Medicine,* vol. 33, pp. 98-101, 2008.

[8]   North Carolina Department of Environment and Natural Resources, Division of Environmental Health, Radiation Protection Section, "The Use and Care of Lead Protective Equipment," *http://www.ncradiation.net/Xray/documents/leadapronsgud.pdf*, Accessed October 2013.

[9]   T. M. Khalil, R. S. Rosomoff, and E. M. Abdel-Moty, *Ergonomics in back pain: a guide to prevention and rehabilitation*, Van Nostrand Reinhold, New York, 1993, pp. 100.

[10]   M. Ross, M. Allan, M. Segal, M. Borenstein, M. Jenkins, and M. Cho, "Prevalence of spinal disc disease among interventional cardiologists," *The American journal of cardiology,* vol. 79, pp. 68-70, 1997.

[11]   P. Lee, V. Shanbhag, and A. Iorwerth, "A simple technique for intra-operative radiation protection in trauma and orthopaedic procedures," *Acta Orthopædica Belgica,* vol. 75, pp. 119-121, 2009.

[12]   H. M. Lederman, Z. P. Khademian, M. Felice, and P. J. Hurh, "Dose reduction fluoroscopy in pediatrics," *Pediatric radiology,* vol. 32, pp. 844-848, 2002.

[13]   M. M. Rehani, "Training of Doctors Using Fluoroscopy," in *World Congress on Medical Physics and Biomedical Engineering, September 7-12, 2009, Munich, Germany*, 2009, pp. 495-497.

[14]   F. H. Raab, E. B. Blood, T. O. Steiner, and H. R. Jones, "Magnetic position and orientation tracking system," *Aerospace and Electronic Systems, IEEE Transactions on,* pp. 709-718, 1979.

[15]   M. A. Nixon, B. C. McCallum, W. R. Fright, and N. B. Price, "The effects of metals and interfering fields on electromagnetic trackers," *Presence: Teleoperators and Virtual Environments,* vol. 7, pp. 204-218, 1998.

[16]   C. Kim, D. Chang, D. Petrisor, G. Chirikjian, M. Han, and D. Stoianovici, "Ultrasound Probe and Needle-Guide Calibration for Robotic Ultrasound Scanning and Needle Targeting," Biomedical Engineering, IEEE Transactions on, vol. 60, pp. 1728-1734, 2013.

[17]   H. Bjartmarz and S. Rehncrona, "Comparison of accuracy and precision between frame-based and frameless stereotactic navigation for deep brain stimulation electrode implantation," *Stereotactic and functional neurosurgery,* vol. 85, pp. 235-242, 2007.

[18]   J. M. Fitzpatrick, J. B. West, and C. R. Maurer Jr, "Predicting error in rigid-body point-based registration," *Medical Imaging, IEEE Transactions on,* vol. 17, pp. 694-702, 1998.

[19]   M. Ghazisaedy, D. Adamczyk, D. J. Sandin, R. V. Kenyon, and T. A. DeFanti, "Ultrasonic calibration of a magnetic tracker in a virtual reality space," in *Virtual Reality Annual International Symposium, 1995. Proceedings.*, 1995, pp. 179-188.

[20]   V. Kindratenko, "Calibration of electromagnetic tracking devices," *Virtual Reality,* vol. 4, pp. 139-150, 1999.

[21]   J. Hong and M. Hashizume, "An effective point-based registration tool for surgical navigation," *Surgical endoscopy,* vol. 24, pp. 944-948, 2010.

요 약 문

경막외강 내시경술 지원 수술 내비게이션 시스템의 개발

경막외강 내시경술은 만성 요통을 수반하는 요추간판탈출 질환에 대한 최소 침습적 치료 시술로써 각광 받고 있다. 하지만 경막외강 내시경술 시술 시 형광투시영상을 사용하여 체강 내 삽입된 카테터의 위치를 확인하기 때문에 방사선 피폭 및 조영제 투여로 인한 부작용을 겪는다는 한계점이 있다. 이에 본 논문에서는 형광투시영상의 대체 및 시술상황의 보다 나은 이해를 돕는 3차원 시각정보의 제공을 목표로 하는 경막외강 내시경술 지원 수술 내비게이션 시스템을 제안한다. 제안된 시스템은 광학식 위치추적장치와 자기장 기반 위치추적장치를 상호보완적으로 함께 사용함으로써 자기장 기반 위치추적장치에 내재하는 낮은 정확도 및 자기장 왜곡에 의한 위치 측정 오차를 보상하고, 제안된 시스템의 내비게이션 정확도를 더욱 향상시키기 위해 다항식 근사에 기반한 자기장 왜곡 보정 방법 또한 적용하였다. 모형 실험을 통해 제안된 시스템의 정확도를 정량적으로 평가하였고, 14회에 걸친 임상 응용을 통해 집도의에 의한 정성적인 평가 또한 이루어졌다.

핵심어: 경막외강 내시경술, 수술 내비게이션, 자기장 왜곡, 캘리브레이션, 좌표계 정합